Title: Collaborative Cross mice have diverse phenotypic responses to infection with Methicillin-resistant *Staphylococcus aureus* USA300.

Short Title: MRSA Infection in CC mice

Authors: Aravindh Nagarajan[1,3], Kristin Scoggin[1,3], Jyotsana Gupta[3], Manuchehr Aminian[6,7], L. Garry Adams[8], Michael Kirby[6], David Threadgill[1,2,4,5], Helene Andrews-Polymenis [1, 3] *

Affiliations

[1]Interdisciplinary Program in Genetics and Genomics, Texas A&M University, College Station, Texas, United States of America

[2]Department of Molecular and Cellular Medicine, Texas A&M University, College Station, Texas, United States of America

[3]Department of Microbial Pathogenesis and Immunology, Texas A&M University, College Station, Texas, United States of America

[4]Texas A&M Institute for Genome Sciences and Society, Texas A&M University, College Station, Texas, United States of America

[5]Department of Biochemistry & Biophysics and Department of Nutrition, Texas A&M University, College Station, Texas, United States of America

[6]Department of Mathematics, Colorado State University, Fort Collins, Colorado, United States of America

[7]Department of Mathematics and Statistics, California State Polytechnic University, Pomona, California, United States of America

22 [8]Department of Veterinary Pathobiology, Texas A&M University, College Station, Texas,
23 United States of America
24
25 *Corresponding author
26
27 Keywords: Host-pathogen interaction, MRSA USA300, Collaborative Cross, QTL
28 mapping, *Npc1*, *Ifi44l*, tolerance, sepsis, sex-difference in infection
29
30

Abstract:

Staphylococcus aureus (*S. aureus*) is an opportunistic pathogen causing diseases ranging from mild skin infections to life-threatening conditions, including endocarditis, pneumonia, and sepsis. To identify host genes modulating this host-pathogen interaction, we infected 25 Collaborative Cross (CC) mouse strains with methicillin-resistant *S. aureus* (MRSA USA300) and monitored disease progression for seven days. We identified eight 'susceptible' CC strains with high bacterial load, tissue damage, and reduced survival. Among the surviving strains, six with minimal colonization were classified as 'resistant', while the remaining six tolerated higher organ colonization ('tolerant'). The kidney was the most heavily colonized organ, but liver colonization was better correlated with reduced survival. We identified four CC strains with sex differences: females survived the study period while males met our euthanasia criteria earlier. In these CC strains, males had more baseline circulating monocytes and red blood cells. We identified several CC strains that may be useful as new models for endocarditis, myocarditis, pneumonia, and resistance to MRSA infection. Resistant strains had higher pre-infection circulating neutrophils than susceptible and tolerant strains. GM-CSF, IL-1-alpha, IL-15, IL-28, and IL-31 levels increased significantly in tolerant strains after infection. Using RNA seq, we identified two pathways, IL-1 and ERK1/ERK2, as potentially involved in the mechanism of tolerance. QTL analysis identified two significant loci, on Chromosomes 18 and 3, involved in early and late survival after infection. We prioritized *Npc1* and *Ifi44l* genes as the strongest candidates influencing survival using variant analysis and mRNA expression data within these intervals.

54 **Importance:**

55 Methicillin-resistant *Staphylococcus aureus* (MRSA) is a human opportunistic pathogen
56 that can cause life-threatening diseases. To study the influence of host genetics on the
57 outcome of MRSA infection, we infected a collection of genetically diverse mice. We
58 identified different phenotypes for survival, organ colonization, and tissue damage, and
59 classified CC strains into MRSA susceptible, tolerant, and resistant categories. Four CC
60 strains had strong sex differences in infection outcome: females lived longer, and males
61 had higher baseline circulating monocytes and red blood cells. Several of the CC strains
62 we characterize may represent better animal models for diseases caused by MRSA.
63 Resistant and tolerant strains appear to have different immunologic states both pre-
64 infection and in response to infection. QTL analysis identified two genes, *Npc1* and
65 *Ifi44l*, as strong candidates for involvement in early and late survival after MRSA
66 infection. Our data suggests a strong involvement of host genetics in MRSA infection
67 outcome.

68

69

70

71

72

73 **Introduction**

74 *Staphylococcus aureus*, a gram-positive pathogen, is a commensal organism
75 and opportunistic pathogen that can cause severe morbidity and mortality [1, 2]. This
76 organism colonizes 20-30% of humans permanently and another 50-60% intermittently
77 [3, 4]. *S. aureus* is a multi-host pathogen that can colonize and cause disease in cows,
78 chickens, pigs, sheep, and wild animals [5]. A range of conditions, from skin and soft
79 tissue infections to severe life-threatening diseases, including sepsis and toxic shock
80 syndrome, can result from *S. aureus* infection [6]. *S. aureus* is the leading cause of
81 bacteremia, skin and soft tissue infections, bone and joint infections, and hospital-
82 acquired infections [7].

83 Methicillin-resistant *S. aureus* (MRSA) is a strain of *S. aureus* resistant to β-
84 lactam, fluoroquinolones, and macrolide antibiotics [8]. Resistance is conferred by the
85 gene 'mecA', acquired by horizontal transfer of a mobile genetic element called
86 Staphylococcal cassette chromosome mec (SCCmec) (Katayama, Ito, & Hiramatsu,
87 2000). MRSA was first described in the early 1960s and was primarily associated with
88 hospital-acquired infections until the 1980s [9, 10]. In the 1990s, MRSA started
89 spreading rapidly in the community and is now considered a global threat [7]. The World
90 Health Organization (WHO) reported that people with MRSA are 64% more likely to die
91 than people with drug-sensitive infections (WHO, 2018). MRSA causes more than
92 300,000 hospitalizations and 10,000 deaths in the US annually, at an estimated
93 healthcare cost of 1.7 billion dollars (CDC, 2018).

94 USA300 is a highly successful community-acquired clone of MRSA. First
95 reported in 1999, by 2011 USA300 had become the primary cause of severe skin and

96 soft-tissue infections, bacteremia, and community-onset pneumonia [11]. The increased
97 disease burden caused by MRSA USA300 is attributed to the presence of multiple
98 mobile genetic elements (MGEs) carrying virulence factors. These virulence factors
99 include Panton-Valentine Leukocidin (PVL) gene, Arginine-Catabolic Mobile Element
100 (ACME), Enterotoxins K and Q, Staphylococcal cassette chromosome *mec* type IV
101 (SCC mec IVa), and fluoroquinolone resistance acquired through mutations in *gyrA* and
102 *grlA* [12, 13]. In humans, USA300 infections are associated with increased mortality and
103 increased incidence of severe sepsis than hospital-acquired MRSA infections [14, 15].
104 This hypervirulence exhibited by USA300 over other strains has been repeatedly
105 demonstrated in several animal models [16-18].

106 Mouse models have helped identify susceptibility genes and understand the
107 mechanism of pathogenesis of many bacterial pathogens and diseases [19]. *S. aureus*
108 infections in mice induce a diverse spectrum of diseases similar to what is observed in
109 humans [20]. Mice lacking MyD88 (myeloid differentiation primary response protein), a
110 cytoplasmic adaptor involved in the IL-1R (Interleukin-1) and TLR-2 (Toll-Like Receptor
111 2) pathways, are highly susceptible to *S. aureus* intravenous infections [21]. Similarly,
112 mice deficient in NOD2 (nucleotide-binding oligomerization domain-containing protein 2)
113 are more susceptible to intraperitoneal infection with *S. aureus* [22].

114 Outcomes after infection with *S. aureus* differ depending on the strain of
115 laboratory mice used. In a bacteremia model, C57BL/6 mice are the most resistant in
116 controlling bacterial growth and survive, while A/J, DBA/2, and BALB/c mice are highly
117 susceptible [23]. This information has been used to map genetic loci involved in this
118 differential outcome. Using C57BL/6J and A/J Chromosomal substitution strains (CSS),

119 six genes on three different chromosomes (Chr 11 – *Dusp3*, *Psme3*; Chr 8 – *Crif1,*
120 *Cd97*; Chr 18 – *Tnfaip8, Seh1l*) have been implicated to susceptibility after infection with
121 *S. aureus* (sanger 476) strain [24-26].

122 Collaborative Cross (CC) mice have been successfully used to create disease
123 models and identify susceptibility genes for various infections [27]. The CC is a large
124 panel of recombinant inbred mouse strains created by interbreeding five classical inbred
125 strains (A/J, C57BL/6J, 129S1/SvlmJ, NOD/ShiLtJ, NZO/HlLtJ) and three wild-derived
126 inbred strains (CAST/EiJ, PWK/PhJ, and WSB/EiJ) using a funnel-breeding scheme
127 [28, 29]. CC strains have more than 30 million Single Nucleotide Polymorphisms
128 (SNPs), and their genomes are fully sequenced, making them an ideal population for
129 Quantitative Trait Locus (QTL) mapping [30, 31]. The CC has been heavily used to
130 identify susceptibility to viral pathogens, including Ebola virus [32], West Nile virus [33],
131 Influenza A virus [34], Coronaviruses [35, 36], Theiler's murine encephalomyelitis virus
132 [37], Cytomegalovirus [38] and Rift Valley fever virus [39]. The CC has also been used
133 to study infection with bacterial pathogens, including *Mycobacterium tuberculosis* [40,
134 41], *Klebsiella pneumonia* [42], *Pseudomonas aeruginosa* [43], *Borrelia recurrentis* [44],
135 *Salmonella* Typhimurium [45, 46] and *Salmonella* Typhi [47].

136 We infected 25 CC strains intravenously with MRSA USA300 to study disease
137 outcomes across diverse host genetics. We monitored infected mice for clinical
138 symptoms using telemetry and a manual health scoring method for up to one-week
139 post-infection. Organs and blood were collected at necropsy to quantify colonization,
140 tissue damage, complete blood counts (CBC), and cytokine levels. We observed a wide
141 range in survival and weight loss after infection. The kidney was the most highly

142 colonized organ, but liver colonization was more highly correlated with poor survival.
143 Four strains exhibited sex differences in survival: infected females lived until the end of
144 the experiment (day 7), but all the males met our euthanasia criteria much earlier.
145 Several CC strains we characterized could be used as new models for studying
146 endocarditis, myocarditis, pneumonia, and resistance to MRSA infection. We also
147 prioritized several blood, cytokines, and immune pathways that differentiated the
148 tolerance from resistance. QTL analysis identified two significant genomic loci involved
149 in early and late survival after infection. Shortlists of the strongest candidate genes
150 within these intervals were generated using variant analysis and mRNA expression
151 data.

152 **Results**

153 CC strains exhibit diverse responses to MRSA infection.

154 We infected twenty-five Collaborative Cross (CC) strains (three males and three
155 females per strain) with MRSA USA300 (Table S1). Animals were monitored for clinical
156 symptoms using a telemetry system and a manual health scoring method up to one-
157 week post-infection to identify those susceptible to MRSA infection. C57BL/6J (B6)
158 mice, known to survive MRSA infection, served as negative controls. At the time of
159 necropsy spleen, liver, heart, lung, and kidney were collected to enumerate the bacterial
160 load (Table S2).

161 All C57Bl6 mice survived until the end of the experiment (day 7) and were
162 classified as a surviving strain (Fig 1A). C57Bl6 mice lost a median of 8.90% of their
163 body weight and had high kidney colonization (Fig 1B and Fig 1C). CC strains that had

164 four or more mice of the six infected meeting our euthanasia criteria before day seven
165 were classified as ‘susceptible’. Eight of the 25 CC strains we infected were classified in
166 this category (CC053, CC027, CC037, CC036, CC061, CC006, CC057, CC002, Fig
167 1A).

168 Five CC strains had three mice that met our euthanasia criteria before day 7. Of
169 these five strains, four showed sex-dependent survival: all the males met our
170 euthanasia criteria early in the experimental period, while all females of these strains
171 survived the full 7-day infection period. These four CC strains were classified as sex-
172 difference strains (CC013, CC058, CC043, CC015, Fig 1A). CC042 couldn’t easily be
173 classified, as two females and one male survived MRSA infection.

174 We classified the remaining 12 surviving CC strains into tolerant and resistant
175 phenotypes. Tolerance was defined as surviving the infection with a high bacterial
176 burden. Surviving the infection by preventing colonization or clearing the pathogen was
177 defined as resistance. Six strains with higher organ colonization compared to the
178 inoculum dose were classified as tolerant (CC019, CC005, CC001, CC024, CC051,
179 CC038). The remaining six strains, with minimal or no colonization, were classified as
180 resistant (CC023, CC025, CC012, CC003, CC041, CC017) (Fig 1 and Fig S1).

181 Pre-infection weight did not influence survival (R = -0.05), while weight loss after
182 infection correlated with poor survival (R = -0.65) (Fig S2). Susceptible strains, on
183 average, lost 16% of their body weight, while tolerant and resistant strains lost 7% and
184 5%, respectively (Fig 1B). Colonization in all five organs was highly correlated (Fig S2).
185 10 mice belonging to 6 different strains had no colonization across the organs collected

186 (Fig 1 and Fig S1). We included them in the analysis based on disturbances in circadian
187 pattern following infection, suggesting that they did become infected as well as histology
188 scores. The kidney was the highest colonized organ across all CC strains and high
189 kidney colonization correlated with poor survival (R = -0.58) (Fig S2). Two susceptible
190 strains, CC027 and CC057, had median kidney colonization on the order of 10^9, ~100-
191 fold higher than the inoculation dose. Several resistant strains, including CC012,
192 CC025, CC003, and CC017, had lower or no MRSA colonization of the kidneys (Fig
193 1C).

194 The inability to limit bacterial growth in the kidney is associated with susceptibility
195 to intravenous *S. aureus* infections in mice [23]. In the CC strains we screened,
196 colonization in the liver (R = -0.78), spleen (R = -0.73), and lung (R = -0.67) was more
197 highly correlated with poor survival than colonization of the kidneys (Fig S2). Heart and
198 kidney colonization were similarly correlated with survival (R = -0.58) (Fig S2).
199 Furthermore, liver colonization had a high positive correlation with the spleen (R = 0.79),
200 lung (R = 0.78), and heart (R=0.67) colonization (Fig S2). These data suggest that
201 several CC strains tolerated high kidney colonization but reached our euthanasia criteria
202 when the pathogen load increased in other organs. The diverse response of CC strains
203 to MRSA infection is evident in the wide range of disease severity, survival, weight loss,
204 and organ colonization we observed.

205 <u>Survival is sex-dependent in four CC strains.</u>

206 A sex difference in survival was defined as only males or females within a strain
207 surviving the infection to day 7. Four strains, CC013, CC015, CC043, and CC058, met

208 this criterion for sex differences (Fig 1A). In these four strains, females lived until the
209 end of the experiment (day 7), but all the males met our euthanasia criteria much earlier
210 (Fig 2A). After removing these four strains and looking at the remaining CC mice (21
211 strains) as a population, there was no significant difference in survival (P = 0.51) and
212 weight change after infection (P = 0.13) between males and females.

213 In the four sex difference strains, males lost more weight than females (Fig 2B)
214 and had higher liver, spleen, and lung colonization (Fig 2C). The colonization did not
215 significantly differ between males and females in the kidneys, the highest colonized
216 organ in these strains (Fig 2C). Females in these CC strains appear to limit MRSA
217 spread from the kidneys and/or bacterial replication in other vital organs by an unknown
218 mechanism.

219 To assess baseline differences between males and females of the sex difference
220 strains, we evaluated pre-infection complete blood counts (CBC). Interestingly, males
221 had higher circulating levels of monocytes and red blood cells before infection than
222 females of these strains (Fig 2D). None of these blood parameters differed significantly
223 between males and females in the rest of the CC population (21 strains). Thus, this
224 difference in the starting blood parameters is unique to CC strains that displayed sex
225 differences in susceptibility to MRSA infection.

226 <u>Tissue damage correlates poorly with survival</u>

227 A board-certified pathologist scored each tissue blindly for damage using a scale
228 of 0 to 4 (0 = normal to 4 = severe damage) (Table S3 and Fig S3). Tissue damage in
229 three of the five organs we examined had a weak correlation with poor survival (Fig S2).

230 Spleen damage had the highest correlation with R = -0.23, followed by the kidney (R = -
231 0.18) and heart (R = -0.18) damage. This weak correlation may be due to the diverse
232 phenotypic responses exhibited by the CC strains to MRSA infection. Some infected CC
233 strains met our euthanasia criteria very early in infection, perhaps before extensive
234 tissue damage had time to occur. Other CC strains lived to the end of the experiment,
235 allowing time for severe tissue damage to occur and become cumulative (Fig 3).

236 However, high colonization in kidneys translated to more significant tissue
237 damage. Of the 25 CC strains we studied, 16 had a median score of 2.5 or above for
238 kidneys, indicating severe tissue damage. Two strains, CC017 and CC043, had no
239 kidney damage (Fig 3). CC017 is a resistant strain explaining minimal tissue damage in
240 the kidneys and other organs. But CC043 had high colonization across all organs and
241 lost more than 10% of their body weight, although this strain had a sex difference with
242 the females resistant to MRSA infection (Fig 1 and S1).

243 For tissue damage, across all the organs, resistant strains had significantly less
244 damage than tolerant strains (P < 0. 001) and susceptible strains (P < 0.010).
245 Interestingly, there was no significant difference in tissue damage as blindly scored by a
246 board-certified pathologist, between tolerant and susceptible strains (P = 0.57). CC042
247 and CC036 mice had severe damage in their hearts. Histologic examination revealed
248 that this damage was purulent bacterial myocarditis and myocardial necrosis. Sex
249 difference strains varied widely in tissue damage scores. Both males and females in
250 CC013 and CC058 had damage across all the tissues, despite the fact that females of
251 these strains survived while the males did not. CC043 did not have any damage in
252 either sex. In CC015, males had more significant kidney damage than females.

253 Baseline body temperature and baseline activity did not correlate with survival.

254 A surgically implanted telemetry device tracked body temperature and activity
255 levels every minute before and throughout the infection. Data from five days before
256 infection was used to create a baseline circadian pattern for each mouse using a
257 machine-learning algorithm. A machine learning algorithm was also used to predict
258 when infected mice deviated from their normal circadian pattern of body temperature
259 and activity after infection. No significant differences were identified in the elapsed time
260 between infection and deviation from the normal circadian pattern between surviving
261 and susceptible strains. 90% of the infected mice deviated from their normal circadian
262 pattern of body temperature and activity within 24 hours of infection (Fig S4). The first
263 health check performed by laboratory staff, 24 hours after infection, could only detect
264 56% of these mice. In the next two days, twice daily health checks detected all the
265 remaining mice as ill (Fig S4). These data suggest a significant lag time between
266 circadian pattern disruption detected by telemetry and signs of illness detected by
267 laboratory staff.

268 Immune parameters that differ between phenotypes.

269 Blood was collected from mice five weeks before the infection by cheek bleed,
270 and at necropsy, whole blood and serum were collected. Complete blood counts (CBC)
271 were determined using an automated CBC machine, and circulating cytokine levels
272 were determined from serum using a 36-plex cytokine/chemokine panel. To account for
273 baseline differences in CBC parameters across the CC strains, we determined the
274 change in each parameter after infection by subtracting post-infection CBC values from
275 pre-infection values from the same animal. Post-infection cytokine/chemokine values

276 were subtracted by values from age and sex-matched uninfected animals from the
277 same CC strains.

278 CC strains resistant to MRSA infection had a higher number of pre-infection
279 circulating neutrophils than susceptible and tolerant strains (Fig 4A). There were no
280 significant differences in other pre-infection CBC parameters. Post-infection, we only
281 looked at the differences between tolerant and resistant strains, as both groups were
282 euthanized at the same time point (Day 7 post infection). Platelet indices, platelet
283 distribution width (PDW), and mean platelet volume (MPV) increased in tolerant strains
284 after infection (data not shown). Increases in these platelet parameters suggest platelet
285 activation is occurring in MRSA tolerant CC strains [48, 49]. Among the 36 cytokines
286 and chemokines we measured, only five differed significantly between the tolerant and
287 resistant strains. GM-CSF, IL-1-alpha, IL-15, IL-28, and IL-31 were significantly elevated
288 in tolerant strains compared to resistant strains (Fig 4B).

289 Kidneys were collected during the necropsy and were used for RNA sequencing.
290 152 genes were differentially expressed between the tolerant and the resistant strains.
291 Of these, 88 were up-regulated in tolerant strains, and 64 were down-regulated (Fig
292 S5A). Differentially expressed genes were analyzed for the enrichment of biological
293 processes. Down-regulated genes were primarily involved in metabolism and electron
294 transport chain, significantly affecting normal cell activities. All up-regulated genes were
295 involved in immune-related pathways (Fig 4C). Homotypic cell-cell adhesion and
296 response to IL-1 were the top two enriched pathways. These processes, up-regulated in
297 tolerant strains, grouped into the ERK1/ERK2 cascade, response to IL-1, response to

298 cytokines, and innate and adaptive immune responses in enrichment tree analysis (Fig
299 S5B).

300 Two independent genomic regions influence survival.

301 We used a modified version of RQTL2 and qtl2qpi to identify chromosomal
302 regions associated with survival after MRSA infection [50, 51]. We used the number of
303 mice within a strain that survived at the end of each day as the phenotype. For a
304 successful QTL analysis, a phenotype needs to be highly heritable. Within the CC
305 strains we infected, survival was a highly heritable trait with a broad sense heritability
306 score of 0.38. When sex was included as a cofactor, heritability increased to 0.63. For
307 early survival on day 2, there was a highly significant peak on chromosome 18 (Fig 5A).
308 We named this QTL peak ESMI (Early Survival in MRSA Infection). This peak
309 disappeared after day 3 post-infection.

310 For survival until day 7 (late survival), there was a highly significant peak on
311 Chromosome 3 (Fig 5B). We named this peak LSMI (Late Survival in MRSA Infection).
312 To understand the impact of sex on survival, we performed the same analysis after
313 removing the four strains that exhibited sex differences in survival. The early survival
314 peak on Chr 18 and late survival peak on Chr 3 were retained (Fig S6), suggesting that
315 sex did not influence our QTL peaks. We compared the phenotype at the top SNPs in
316 both peaks for potential interaction. We did not identify any significant interactions,
317 suggesting that our QTL regions act independently of each other.

318 *Npc1* is a candidate gene for early survival during MRSA infection.

319 The advantage of CC panel over other outbred mouse panels is the high number
320 of SNPs and structural variants present across the CC genomes [30, 31]. We used this
321 feature to shortlist the genes within the associated genomic regions to identify those of
322 most interest. The early survival QTL peak, ESMI, on chromosome 18 is a 5 Mb region
323 between 12-17 Mb with a peak around 14.67 Mb. This region contains 21 protein-coding
324 genes and 49 non-coding RNA genes. Because the CC strains are a mosaic of eight
325 inbred founder strains, we looked at the founder effect plot in this region to attempt to
326 identify each founder's contribution to survival. We found that the WSB allele
327 contributes to reduced survival, while A/J and NZO alleles contribute to prolonged
328 survival (Fig 6A). Using all the SNPs and indels that matched this allele effect pattern
329 using the Mouse Phenome Database (MPD), we identified 20,582 variants spread
330 across all 21 genes. We used Variant Effect Predictor (VEP) to further prioritize these
331 variants based on their predicted effect on protein structure and function, identifying 52
332 high and moderate-impact variants in 7 genes (Table S4). The highest impact variant
333 for each gene is listed (Fig. 6B). Four of the seven genes we shortlisted have previously
334 been associated with immune function in the Mouse Genome Informatics Portal
335 (highlighted in red) [52]. We sequenced mRNA from kidneys collected from CC strains
336 at necropsy (at least one male and one female per strain) to further prioritize genes.
337 Then, we looked for differentially expressed genes that matched the founder effect
338 pattern within this region. For the early survival QTL peak, two genes, *Npc1* and *Cdh2*,
339 matched the founder effect pattern (Fig 7C). *Npc1* is our top candidate in this region due
340 to its previous association with the immune system.

341 <u>*Ifi44l* is a strong candidate for involvement in late survival after MRSA infection.</u>

342 The late survival QTL peak, LSMI, on chromosome 3 is a 4 Mb region between
343 146-150 Mb with a peak near 146.66 Mb. This region contains 13 protein-coding genes
344 and 39 non-coding RNA genes. The A/J allele significantly reduced survival, while
345 CAST, NOD, NZO, and WSB alleles promoted longer survival (see founder effect plot,
346 Fig 7A). Using this founder effect pattern, we shortlisted five genes with variants
347 predicted to have a high impact on the function of the encoded proteins (Table S4). The
348 top variant for each gene is listed (Fig 7B). Gene expression data narrowed our shortlist
349 to *Ifi44l*, a gene that is highly expressed in strains with the A/J allele but not with the
350 alleles from the other founders (Fig 7C).

351 <u>QTL analysis for other phenotypes.</u>

352 We collected a large amount and variety of data throughout this experiment and
353 wanted to utilize as much of this data as possible. Therefore, in addition to using the
354 survival data, we performed QTL analysis for 188 other phenotypes. These phenotypes
355 included weight change, circadian parameters, nestlet scores, CBC, and
356 cytokine/chemokine values, before and after MRSA infection. At an 85% significance
357 level, we detected 39 QTL peaks for 36 parameters (Table S5). The median 1.8 drop
358 interval for these peaks was 6.12 Mb. We focused on the 15 peaks that passed the
359 significance at the 95 % level for variant shortlisting (Table S5). We generated the
360 founder effect and phenotype-genotype plot for each QTL peak (Fig S7). Using the
361 Mouse Phenome Database (MPD), we shortlisted high-impact genes in these intervals
362 that matched the founder effect pattern (Table S6).
363

364

365 **Discussion**

366 *Staphylococcus aureus* (*S. aureus*) is a highly successful organism that
367 colonizes approximately one-third of the human population asymptomatically [3]. *S.*
368 *aureus* colonization is a risk factor for subsequent infections ranging from mild skin and
369 soft tissue infections to serious invasive infections and death [53, 54]. *S. aureus* has a
370 complex repertoire of virulence factors, pathogenicity islands, and toxins and has
371 developed resistance to multiple antibiotics [9]. Many studies have focused on
372 understanding the genetics of *S. aureus* pathogenesis, but the host genetic factors that
373 may modulate this host-pathogen interaction are poorly studied. We infected 25
374 genetically diverse CC mouse strains with MRSA USA300 to find the host genetic
375 factors contributing to disease susceptibility or resistance over a 7-day infection.

376 CC strains vary widely in their response to MRSA sepsis. Survival ranged from
377 2.5 to 7 (end of the experiment) days. Weight loss ranged from strains losing 20% of
378 their body weight (CC037, CC002) to strains losing less than 1% (CC017, CC003,
379 CC024). The kidney is one of the primary organs for MRSA colonization in mice and
380 was the highest colonized organ in our study [23, 55]. However, across CC strains,
381 kidney colonization varied widely. Some strains (CC003, CC041, CC017) had minimal
382 or no colonization, but others had very high colonization (CC057, CC027) (Fig 1C). In
383 CC strains, high liver, spleen, and lung colonization correlated more closely with poor
384 survival than did kidney colonization (Fig S2). Kupffer cells, specialized liver
385 macrophages, are essential for the initial clearing of *S. aureus* from the bloodstream
386 [56, 57]. Perhaps high MRSA colonization in the liver overwhelms the ability of resident

387 Kupffer cells to clear MRSA, contributing to the correlation between liver colonization
388 correlates and poor survival in CC strains.

389 We identified 8 CC strains that were susceptible to MRSA sepsis based on
390 reduced survival after infection. Within these susceptible strains, the phenotypic
391 response was diverse. Survival ranged from 2.5 to 4 days, and kidney colonization
392 ranged from 2 $x10^8$ to 2 $x10^9$ CFU/g of tissue (Fig 1A). CC061 (3.3 $x10^8$ CFU/g) and
393 CC036 (2.37 $x10^8$ CFU/g) had very similar kidney colonization, yet CC061 appeared to
394 have a more severe disease as they lost double the amount of body weight of CC036
395 (19% vs. 9%) (Fig 1B and 1C). We observed similar diversity in weight loss and
396 colonization within tolerant and resistant phenotypes as well. These data suggest CC
397 strains may each have a distinct mechanism leading to susceptibility or survival.

398 The majority of the CC strains used in this study were also used to define
399 susceptibility to non-typhoidal *Salmonella* infection [45, 46]. Of the eight MRSA
400 susceptible strains, six were also classified as susceptible or delayed susceptible to
401 *Salmonella* infection (CC053, CC027, CC037, CC036, CC061, CC006). The two
402 remaining MRSA susceptible strains, CC057 and CC002, were classified as resistant
403 and tolerant to *Salmonella* infection, respectively [46]. CC038 was classified as tolerant
404 to both MRSA and *Salmonella* infection. None of the other MRSA tolerant or resistant
405 strains matched the *Salmonella* classification.

406 We also compared MRSA infection outcome data to another study of
407 *Mycobacterium tuberculosis* (Mtb) infection in CC strains [41]. This study did not classify
408 survival phenotypes, so we used the median lung colonization values for each strain for
409 comparison to our survival data. For the 52 CC strains infected with Mtb, log lung CFU

410 ranged from 5.1 to 8.5, with a median of 6.7 CFU. Among the six MRSA-susceptible
411 strains, two strains, CC061 and CC006, had very low lung CFU (5.6 and 6.5 log CFU)
412 when infected with *Mtb*. On the other hand, three other susceptible strains, CC037,
413 CC027, and CC002, had very high lung colonization with *Mtb* (average – 8.2 log CFU).
414 Two of these strains, CC027 and CC037, were sensitive to both *Salmonella* and MRSA
415 infection and were also heavily colonized in the lung with *Mtb* [41, 45, 46]. These data
416 suggest that in these two CC strains, sensitivity to three different bacterial pathogens
417 may be occurring through a common mechanism.

418 All five MRSA-resistant CC strains when infected with *Mtb* had very high
419 colonization in the lung (average – 8.4 log CFU), suggesting these strains were likely
420 susceptible to *Mtb* infection. CC038, classified as tolerant to MRSA and *Salmonella*, is
421 also likely tolerant to *Mtb* infection with a lung CFU of 7.3, close to the median lung
422 colonization across all CC strains. The other MRSA-tolerant strains had variable *Mtb*
423 CFU in the lungs. This differential response of CC strains to different bacterial
424 pathogens suggests that most CC strains that we used do not have a significant general
425 dysfunction of immunity, where we would expect broad susceptibility to multiple
426 pathogens.

427 In both animals and humans, males are more susceptible than females to
428 bacterial infections [58]. Some of these differences can be attributed to the differences
429 in X-chromosome number and inactivation process between males and females. The X-
430 chromosome also encodes several critical immune genes, including interleukin-1 (IL-1)
431 receptor-associated kinase 1 (IRAK1), Colony-stimulating factor 2 receptor α (CSF2RA),
432 IL-2 receptor-γ chain, IL-3 receptor-α chain, IL-9 receptor, Toll-like receptor 7 (TLR7),

433 TLR8, and FOXP3, that could play important roles in sex differences in infection
434 outcome [59]. Males have a higher overall risk for MRSA carriage [60] and bloodstream
435 infections [61, 62]. However, there is no consensus on the role of gender in the mortality
436 rate. Several studies have found higher mortality in females [63-65], while other studies
437 have reported no association of mortality with gender [62, 66].

438 In our total study population, females survived longer than males ($P < 0.01$).
439 However, this survival difference was driven by 4 CC strains that exhibited strong sex
440 differences in survival. Within the strains with sex differences in survival, males lost
441 more weight and were colonized more heavily in the liver, spleen, and lung than females
442 (Fig 2C and 2D). We examined the blood parameters of male and female uninfected
443 mice of these CC strains to identify baseline differences. Two blood parameters,
444 circulating monocytes (MON) and red blood cells (RBC), were higher in males of these
445 strains prior to infection (Fig 2D) but were not significantly different between the sexes
446 in the rest of the CC population.

447 While the reason why these blood parameters vary must be further investigated,
448 *S. aureus* has a repertoire of virulence factors to take advantage of these parameters in
449 males. *S. aureus* persists within monocyte-derived macrophages and can use these
450 cells as a vehicle for further dissemination [67, 68]. Similarly, S *aureus* can bind directly
451 to both RBCs [69-71] and hemoglobin [72] and possesses multiple virulence factors to
452 lyse erythrocytes [73]. Additionally, heme iron is the preferred source of iron for *S.*
453 *aureus* during infection [74]. Increased pre-infection levels of monocytes may serve as a
454 mechanism for more efficient MRSA dissemination and increased RBC and hemoglobin
455 may serve as nutrient source during infection in males of some CC strains.

456 One of the advantages of using a panel of genetically diverse inbred mice is the
457 ability to identify mouse strains for model generation. MRSA is well adapted to multiple
458 hosts and can cause diverse diseases but studying these diseases in humans is heavily
459 confounded by environmental factors and comorbidities [20, 75, 76]. Thus, studies
460 investigating the pathogenesis of *S. aureus* have relied heavily on mouse models [77].
461 The four sex-difference strains we identified are ideal candidates for investigating the
462 role of sex/gender in MRSA infection outcomes.

463 *S. aureus* is the leading cause of infective endocarditis (IE), which results in high
464 mortality (40-50%) [78, 79]. Current mouse models of IE involve anesthetizing mice and
465 physically damaging the heart valve using a catheter prior to *S. aureus* infection [80].
466 C57BL6 mice are typically used as background strains for the IE model [81]. *S. aureus*
467 is also the most common cause of rare bacterial myocarditis, with fatal outcomes in
468 some cases [82-84]. Currently, there are no murine models to study MRSA induced
469 myocarditis. In our study, three CC strains, C0042, CC013, and CC036, had over 200-
470 fold greater colonization in the heart compared to C57BL6 mice (Fig S1C). CC042 and
471 CC013 also had severe tissue damage in the heart (Fig 3). On histological examination,
472 we observed systemic embolic bacterial purulent myocarditis (Fig S3). CC042 and
473 CC013 may make better, simpler inbred mouse models for studying cardiac disease
474 due to MRSA without the need to physically damage heart valves prior to infection.

475 Similarly, pneumonia caused by *S. aureus* has a high mortality rate [85]. In our
476 study, three strains, CC013, CC058, and CC061, had significant damage in the lung
477 (Fig 3) and could be used for studying *S. aureus* pneumonia. C57BL6 mice are the most
478 resistant mouse strain to *S. aureus* infection in the literature [23, 26], but do not clear

479 the pathogen completely. We identified six resistant CC strains that both survive MRSA
480 infection and have lower bacterial colonization than C57BL6 mice (Fig 1 and S1). Most
481 of these strains also had less tissue damage than C57BL6 mice (Fig 3). These resistant
482 strains are ideal candidates for future studies investigating the mechanisms of
483 resistance to *S. aureus* infections.

484 Changes in body temperature and activity are important clinical signs for disease
485 diagnosis and prognosis. During the recent COVID-19 pandemic, there was an
486 increased emphasis on using changes in body temperature to detect illness all over the
487 world [86, 87]. The reliability of using body temperature to screen patients with COVID-
488 19 illness has been questioned [88, 89]. Using an implanted telemetry device, we
489 measured the core body temperature and activity of each animal in our study. Daytime
490 baseline body temperature strain medians varied from 35.81 C to 37.14 C (96.46 F-
491 98.85 F), and nighttime temperature varied from 36.41 C to 37.61 C (97.54 F - 99.70 F)
492 (Table S2). Similarly, the difference between the night (active) and day (resting)
493 temperatures varied from 0.3 C to 0.9 C (0.5 F - 1.6 F). The diversity in these thermal
494 regulation patterns across CC strains should prompt caution when interpreting a single
495 measurement of body temperature as an indicator of illness in mice. Both pre-infection
496 temperature and activity were highly heritable (Temperature – day = 0.59, night = 0.60,
497 Activity – day = 0.72, night = 0.61), suggesting the involvement of a genetic component.
498 Unfortunately, we did not identify significant peaks in our QTL analysis for these
499 parameters. In the future, adding more CC strains to this analysis may help identify the
500 genetic loci that influence body temperature and activity. Accounting for genetic
501 variation in body temperature measurements should improve the accuracy of using

502 body temperature as a screening tool for detecting illnesses particularly in laboratory
503 animals.

504 Pre-infection inflammation and immune parameters play a role in disease
505 prediction and progression [36, 90]. Among all the CBC parameters we compared, pre-
506 infection circulating neutrophil numbers were significantly higher in MRSA resistant
507 strains than in the tolerant and susceptible strains (Fig 4A). Neutrophils are the primary
508 defense against *S. aureus* infections [54, 91]. Patients with impaired neutrophil numbers
509 and function are predisposed to *S. aureus* infections [92-94]. The high pre-infection
510 circulating neutrophil numbers in the MRSA-resistant CC is consistent with this human
511 data and may decrease colonization by MRSA in these strains.

512 *S. aureus* evades phagocytosis by modifying its cell surface and producing a
513 repertoire of virulence factors [95, 96]. These factors aid in both evading and attacking
514 the host immune system. We found increases in GM-CSF, IL-1α, IL-15, IL-28, and IL-31
515 levels in tolerant strains compared to the resistant strains. GM-CSF and IL-1α recruit
516 neutrophils and upregulate their properties to clear pathogens [97-99]. Tolerant strains
517 appear to be actively recruiting neutrophils to clear MRSA.

518 However, IL-28, IL-15, and IL-31 may help *S. aureus* persist, but these effects
519 have not been demonstrated in models of septic infection. Mice lacking the receptor for
520 IL-28 clear *S. aureus* better and have less pulmonary pathology [100]. Similarly, mice
521 lacking IL-15 have improved clearance of *S. aureus* in a mouse arthritis model [101],
522 and IL-31 supplementation enhanced *S. aureus* colonization in an epidermal model
523 [102]. Further studies will tease out the role of these cytokines in the tolerance
524 phenotype during sepsis.

525 The two pathways up-regulated in tolerant strains in our gene expression
526 analysis are IL-1 and the ERK1/ERK2 cascade (Fig 4C and S4B). In humans, mutations
527 in the IL-1 pathway lead to increased susceptibility to some bacterial infections,
528 particularly streptococcal and staphylococcal infections [103]. Activation of the IL-1
529 receptor (IL-1R) via the secretion of IL-1α and IL-1β activates the MyD88/IRAK4
530 pathway, resulting in the production of cytokines and chemokines promoting neutrophil
531 recruitment and pathogen clearance [104]. In *S. aureus* septic infections, IL-1R deficient
532 mice have increased mortality [105], and blocking the IL-1 receptor increased
533 susceptibility in mice [98]. In our experiments, IL-1α levels are increased in the serum of
534 tolerant strains (Fig 4B). Thus, the IL-1 pathway appears to play a critical role in the
535 survival of MRSA-tolerant strains, potentially causing increased neutrophil recruitment.

536 The extracellular signal-regulated kinase 1/2 (ERK1/2) signaling pathway
537 regulates cell proliferation, differentiation, and survival during stress response [106].
538 ERK1/2 molecules are expressed in very large quantities (~10^7 molecules/cell) and bind
539 more than 200 distinct substrates in the cell [107]. Although ERK 1/2 enters the nucleus
540 and alters gene expression of several transcription factors, including NF-κB, its role in
541 bacterial infections is poorly understood [108]. ERK1/2 inhibitors have been successfully
542 used to increase survival in mouse models of *S. aureus* sepsis [109, 110], but their
543 mechanism of action is not clearly known. Future studies will be needed to identify the
544 mechanism of ERK1/2 pathway participation in the tolerance phenotype.

545 Survival of MRSA infected mice lasted from two to seven days and was
546 considered a complex trait for QTL analysis. For early survival, there was a significant
547 peak on Chromosome 18. This peak was significant at the 0.95 permutation threshold

548 and contained 21 protein-coding genes. The WSB allele at this locus contributed to
549 shorter survival. Seven genes in this region have mutations that have a predicted high
550 impact on protein function. While any of these variants could contribute to the reduced
551 survival phenotype, based on mRNA expression data we collected, we focused on
552 Cadherin2 (*Cdh2*) and NPC intracellular cholesterol transporter 1 (*Npc1*).

553 Chd2 encodes N-cadherin, which mediates calcium-dependent cell-cell adhesion
554 [111]. In humans, *CDH2* variants are associated with arrhythmogenic right ventricular
555 cardiomyopathy (ARVC) [112, 113]. In mouse models, *Cdh2* conditional knockouts have
556 abnormal heart structure and function [114]. *S. aureus* manipulates cell-cell adhesion for
557 biofilm formation [115] and changes in the cardiac wall structure to invade tissues [81].
558 *S. aureus* may use abnormalities in the cardiac wall structure created by the WSB *Cdh2*
559 variants to colonize early in infection.

560 The primary candidate gene in this QTL, *Npc1*, is present in the membrane of
561 endosomes and lysosomes and mediates intracellular cholesterol trafficking [116]. In
562 humans, mutations in *NPC1* cause Niemann–Pick Type C disease, leading to massive
563 accumulation of cholesterol in lysosomes in all tissues and premature death [117].
564 Defects in *Npc1* can lead to increased lipid storage in macrophages and a chronic
565 inflammatory condition [118, 119]. NPC1 is also the primary host factor responsible for
566 Ebola, and other filovirus, entry into the cell [120]. These viruses use the *Npc1* receptor
567 in endosomes and lysosomes to trigger a membrane fusion process that allows the
568 expulsion of the viral genome into the cytoplasm and subsequent viral replication [121].
569 *Npc1* also plays an important role in Human Immunodeficiency virus type-1 (HIV-1)
570 [122], Hepatitis C virus [123] and Chikungunya virus infections [124].

571 Little is known about the role of *Npc1* in bacterial infections. In a hematopoietic
572 mouse model, *Npc1* mutant mice have a significant increase in the relative abundance
573 of *Staphylococcus* ssp. in their intestine [125], suggesting a role for *Npc1* in keeping
574 *Staphylococcus* ssp. at a low level in this niche. Mutations in *Npc1* impair steady-state
575 autophagosome maturation and interfere with the autophagic trafficking of bacteria to
576 lysosomes in macrophages [126]. *S. aureus* manipulates autophagy in both neutrophils
577 and macrophages to promote its survival and escape [127] [128, 129]. In a large human
578 GWAS study, several SNPs within the *Npc1* gene are associated with changes in
579 neutrophil counts, linking this gene to neutrophil abundance (n = 173,480) [130]. CC
580 mouse strains carrying the WSB allele of *Npc1* have a missense mutation. This altered
581 form of *Npc1* may interfere with autophagy in macrophages and neutrophils, such that
582 *S. aureus* can survive initial phagocytosis leading to the early susceptibility phenotype.

583 The A/J allele on Chromosome 18 contributed to reduced survival of MRSA
584 infected mice on day 7. A/J mice are highly susceptible to a different strain of *S. aureus*
585 (SH1000) [23]. Among the 13 protein-coding genes with high impact variants in this
586 region, five matched the founder effect allele pattern. *Ifi44* and *Ifi44l* are our primary
587 candidates at this locus. *Ifi44* has a missense mutation, and *Ifi44l* has a high-impact
588 variant in the gene's promoter region. In mice and humans, *Ifi44l* is a paralog of *Ifi44*
589 and belongs to the Interferon stimulated gene (ISG) family. Both these genes encode
590 proteins with similar size and sequence identity, but it is unclear if they have redundant
591 or distinct functions [131].

592 Since there was no difference in mRNA expression for *Ifi44* between the founder
593 genotypes, we focused on *Ifi44l*, which was expressed significantly higher in strains with

594 A/J backgrounds. *Ifi44l* promotes macrophage differentiation during bacterial infection
595 and facilitates inflammatory cytokine secretion [132]. Overexpression of *Ifi44* or *Ifi44*L
596 was sufficient to control respiratory syncytial virus (RSV) infection [131]. *Ifi44l* represses
597 the interferon response, protecting the host from the negative effects of the innate
598 immune response during viral infection [133]. The A/J *Ifi44l* allele may be less effective
599 in controlling the interferon response, reducing the survival of *S. aureus* infected mice in
600 the later stages of infection.

601 Ours is the first study of the effects of host genetic variation during MRSA
602 USA300 sepsis in a genetically diverse inbred mouse panel. A series of previous studies
603 examined the genetic differences that influence *S. aureus* (strain Sanger-476) infection
604 in A/J and BL/6 mice using a chromosome substitution strain (CSS) model [24-26]. Six
605 genes belonging to three different chromosomes (Chr 11 – *Dusp3, Psme3*; Chr 8 –
606 *Crif1, Cd97*; Chr 18 – *Tnfaip8, Seh1l*) were implicated in susceptibility after infection
607 with *S. aureus*. The mechanism of susceptibility in A/J mice was attributed to increased
608 inflammation and a decreased immune response in response to *S. aureus* infection [24].

609 We did not identify any genes in common with this previous work, likely due to
610 the differences in both the pathogen and the mouse strains used in both studies [24].
611 Like USA300, Sanger-476 is a community-acquired strain collected in the United
612 Kingdom but is sensitive to methicillin [134]. USA300 also has additional pathogenicity
613 islands, including SaPI5 and SaPIm4, that are absent in the Sanger-476 strain [135].
614 During infection, USA300 also produces higher amounts of virulence factors compared
615 to other MRSA strains [16, 136, 137]. These genetic differences make USA300 distinct
616 from, and potentially more virulent than, other community-acquired clones of MRSA. On

617 the host side, CC founders include six additional inbred strains (three wild-derived),
618 making the collection of CC strains more genetically diverse than the CSS panel.
619 However, given that studies using the CSS panel identified increased inflammation and
620 defective immune responses as critical to MRSA resistance, we were encouraged to
621 see the mutations in the genes we shortlisted (*Npc1*, *Ifi44l*) also contribute to increase
622 inflammation and a defective immune response.

623 Using survival, colonization, telemetry, and histology data, we show the diversity
624 underlying the host response to MRSA USA300 infection. We successfully classified CC
625 strains into susceptible, resistant, and tolerant phenotypes with respect to MRSA
626 infection and identified several immune factors that may moderate these phenotypes.
627 We also described MRSA models for studying sex differences, resistance, MRSA
628 mediated heart damage, and pneumonia. We identified pathways, IL-1, and ERK1/2,
629 that could be involved in the mechanisms of tolerance to MRSA infection. Finally, we
630 have described two novel genomic regions that influence early and late survival after
631 MRSA infections. With several *S. aureus* vaccines failing at human clinical trials [138,
632 139], our data support strong consideration of host genetics as an important factor while
633 designing therapeutics and vaccines against pathogens.

634

635 **Materials and Methods**

636 Ethics statement

637 All mouse studies followed the Guide for the Care and Use of Laboratory of
638 Animals of the National Institutes of Health. The animal protocols (2015-0315 D and

639 2018-0488 D) were reviewed and approved by Texas A&M Institutional Animal Care and
640 Use Committee (IACUC).

641 Bacterial strains and media

642 Methicillin-resistant *Staphylococcus aureus* isolate (USA300) used in this study
643 was the kind gift of Dr. Magnus Hook (Texas A&M Institute of Biosciences and
644 Technology, Houston). USA300 is a fully virulent, community-acquired clone of MRSA.
645 Strains were routinely cultured in Luria-Bertani (LB) broth and plates supplemented with
646 antibiotics when needed at 50 mg/L Kanamycin Sulphate. For murine infections, strains
647 were grown aerobically at 37^0C to a stationary phase in LB broth supplemented with
648 Kanamycin.

649 Murine strains

650 Both conventional (C57BL/6J) and Collaborative Cross (CC) mice were used for
651 these experiments. In total, three males and three females belonging to 25 different CC
652 strains and C57BL/6J (156 mice) were used. All mice were initially purchased from
653 UNC's Systems Genetics Core Facility (SGCF). They were bred independently at the
654 Division of Comparative Medicine at Texas A&M University (Table S1). Mice were fed
655 Envigo Teklad Global 19% Protein Extrudent Rodent Diet (2919) or Envigo Teklad
656 Rodent Diet (8604) based on strain need. Mice were provided with cardboard huts,
657 food, and water ad libitum.

658 Placement of telemetry devices

659 Mice (5-7 weeks old) were anesthetized with an isoflurane vaporizer using the
660 Kent Scientific SomnoSuite Low-flow anesthesia system to implant telemetry devices. A

661 midline abdominal incision was made, and Starr Life Science G2 Emitter devices were
662 sutured to the ventral abdominal wall. The abdominal muscle layer was sutured with 5-0
663 vicryl, and the skin layer was closed using stainless steel wound clips. Buprenorphine
664 (0.0001 mg/g) was administered intraperitoneally before recovery from anesthesia. Mice
665 were monitored twice daily for surgical complications and humanely euthanized when
666 needed. Surgical clips were removed on the seventh day, and animals were allowed to
667 recover for one more week.

668 Health monitoring

669 After the recovery from surgery, mice were moved to a BSL-2 facility and
670 acclimated for 5-7 days. Individual cages containing implanted mice were placed onto
671 ER4000 receiver platforms and calibrated to receive signals from the implanted
672 telemetry devices. The outputs, body temperature (once per minute) and gross motor
673 activity (summation of movement per minute), were continuously fed to a computer
674 system for visualization (Fig S8 and Fig S9). We manually scored four health
675 parameters twice daily: physical appearance, body conditioning, and provoked and
676 unprovoked behavior. The scoring scale ranged from 0-3, with zero = normal and three
677 = abnormal. Additionally, as a measure of activity, four small nestlets were placed at
678 each corner of the cage in the evening. The following day, the number of nestlets moved
679 from the cage corners into the hut was noted.

680 Infection with MRSA

681 After baseline scoring for health, mice (now 8-12 weeks old) were infected with
682 MRSA USA300. Briefly, Mice were anesthetized using isoflurane and infected with 1 x

683 10^7 CFU in 50 µl of LB broth intravenously at the inferior fornix into the retro-orbital
684 sinus. Mice that became moribund within 6 hours of infection were humanely
685 euthanized and removed from the experiment.

686 Bacterial load determination

687 After infection, mice were monitored continuously using telemetry readings and
688 twice daily using visual health scoring. Mice that developed illness as measured by
689 telemetry and our scoring criteria were humanely euthanized by CO2 asphyxiation. After
690 euthanasia, whole blood, serum, and organs (spleen, liver, heart, lung, and kidney)
691 were collected. A consistent region of each organ was collected in 3mL ice-cold PBS
692 and homogenized. The serially diluted homogenate was plated on LB plates
693 supplemented with kanamycin for bacterial enumeration in each organ. Data are
694 expressed as CFU/g of tissue.

695 Identification of deviation from the circadian pattern of body temperature and activity

696 A machine learning algorithm was used to identify the deviation from the
697 circadian pattern of boy temperature and activity. Detailed explanation of the
698 methodology and calculations can be found here [45].

699 Histopathology

700 After euthanasia, portions of collected organs were fixed in 10% neutral buffered
701 formalin for 24 hours and stored in 70% ethanol. Fixed tissue was embedded in paraffin,
702 sectioned at 5 µm, and stained with hematoxylin and eosin (H&E). A board-certified
703 veterinary pathologist scored all the slides for tissue damage on a scale of 0 to 4 in a
704 blinded manner (Table S3). Whole slide images of H&E-stained tissue sections were

705 captured as digital files by scanning at 40X using a 3D Histech Pannoramic SCAN II FL
706 Scanner (Epredia, MI). Digital files were processed by Aiforia Hub (Cambridge, MA)
707 software to generate images with scaled bars.

708 Complete blood count

709 One week before the implantation of telemetry devices, whole blood was
710 collected from each mouse by submandibular bleeding. From the same mice, blood was
711 collected at necropsy after infection by cardiac puncture. Abaxis VetScan HM5,
712 optimized for rodents, was used to analyze blood collected in Ethylene Diamine Tetra
713 Acetic acid (EDTA) tubes. The difference between the blood parameters after and
714 before infection (positive value = increased after infection and negative value =
715 decreased after infection) was calculated and reported.

716 Cytokine and chemokine analysis

717 Serum was separated from the whole blood collected at necropsy. Invitrogen
718 ProcartPlex Cytokine/Chemokine Panel 36 plex kit was used to analyze the serum as
719 per manufacturer instructions. Briefly, magnetic beads were added to each well of the
720 96-well plate and washed with a wash buffer. 25 ul of serum from each mouse was
721 added in duplicates to the plates along with the standards provided in the kit. After
722 shaking for an hour, 25ul of detection antibody was added to the plates and incubated
723 for 30 minutes. This was followed by adding 50 ul of SAPE for 30 minutes, washing, and
724 120 ul of reading buffer to each well. The kit screens for the following 36 cytokines and
725 chemokines: IFN gamma; IL-12p70; IL-13; IL-1 beta; IL-2; IL-4; IL-5; IL-6; TNF alpha;
726 GM-CSF; IL-18; IL-10; IL-17A; IL-22; IL-23; IL-27; IL-9; GRO alpha;IP-10; MCP-1; MCP-

727 3; MIP-1 alpha; MIP-1 beta; MIP-2; RANTES; Eotaxin; IFN alpha; IL-15; IL-28; IL-31; IL-
728 1 alpha; IL-3; G-CSF; LIF; ENA-78/CXCL5; M-CSF. Average values from the duplicates
729 were used for the analysis. To obtain pre-infection levels, serum was collected from
730 age-matched uninfected mice and run using the same protocol mentioned above. The
731 median values of uninfected animals for each strain were used as the baseline for that
732 strain. The difference between infected and uninfected animals (positive value =
733 increased after infection and negative value = decreased after infection) was calculated
734 and reported.

735 QTL analysis

736 QTL analysis was performed using R/qtl2 software [50]. This method accounts
737 for the complex population structure in CC strains. Briefly, genome scans were
738 performed on the transformed phenotype and genotypes imputed from the QTL viewer.
739 The generated Logarithm of Odds (LOD) score is the likelihood ratio comparing the
740 hypothesis of a QTL at a given position versus that of no QTL. Each phenotype was
741 randomly shuffled 999 times to establish genome-wide significance, and LOD scores
742 were calculated for each iteration. The 85th percentile of the scores was considered
743 significant for that phenotype. The genomic confidence interval was calculated by
744 dropping the LOD scores by 1.8 for each significant peak. Mouse Genome Informatics
745 (MGI) was used to find the genes and QTL features within each interval [140]. To further
746 shortlist candidate genes, the founder strain distribution pattern was queried against the
747 CC variant database (V3 Version). The Variant effect predictor [VEP] from the ensemble
748 genome database was used to calculate the impact score for the variants [141].

749 RNA extraction and sequencing

750 Total RNA was extracted from frozen tissues using Direct-zol RNA Miniprep plus
751 kit following the manufacturer's protocol (Zymo Research - R2073). The purity and
752 quantity of the extracted RNA were analyzed using RNA 6000 Nano LabChip Kit and
753 Bioanalyzer 2100 (Agilent CA, USA, 5067-1511). High-Quality RNA samples with RIN
754 number > 7.0 were used to construct the sequencing library. After total RNA was
755 extracted, mRNA was purified from total RNA (5ug) using Dynabeads Oligo (dT) with
756 two rounds of purification (Thermo Fisher, CA, USA). Following purification, the mRNA
757 was fragmented into short fragments using divalent cations under elevated temperature
758 (Magnesium RNA Fragmentation Module (NEB, cat. e6150, USA) under 94℃ 5-7min).
759 Then the cleaved RNA fragments were reverse-transcribed to create the cDNA by
760 SuperScript™ II Reverse Transcriptase (Invitrogen, cat. 1896649, USA), which were
761 next used to synthesize U-labeled second-stranded DNAs with E. coli DNA polymerase
762 I (NEB, cat.m0209, USA), RNase H (NEB, cat.m0297, USA) and dUTP Solution
763 (Thermo Fisher, cat. R0133, USA). An A-base was then added to the blunt ends of each
764 strand, preparing them for ligation to the indexed adapters. Each adapter contained a T-
765 base overhang for ligating the adapter to the A-tailed fragmented DNA. Dual-index
766 adapters were ligated to the fragments, and size selection was performed with
767 AMPureXP beads. After the heat-labile UDG enzyme (NEB, cat.m0280, USA) treatment
768 of the U-labeled second-stranded DNAs, the ligated products were amplified with PCR
769 by the following conditions: initial denaturation at 95℃ for 3 min; 8 cycles of
770 denaturation at 98℃ for 15 sec, annealing at 60℃ for 15 sec, and extension at 72℃ for
771 30 sec; and then final extension at 72℃ for 5 min. The average insert size for the final
772 cDNA libraries was 300±50 bp. At last, we performed the 2×150bp paired-end

773 sequencing (PE150) on an Illumina Novaseq™ 6000 following the vendor's
774 recommended protocol.

775 RNA sequencing data analysis

776 Reads were trimmed using trim galore (version 0.6.7) [142-145]. This removed
777 adapters, poly tails, more than 5% of unknown nucleotides, and low-quality reads
778 containing more than 20% of low-quality bases (Q-value <20). Both forward and reverse
779 hard trimmed at 100 base pairs. FastQC was used to verify data quality before and after
780 cleaning [145]. Cleaned reads were aligned and counted against the mouse reference
781 genome (GRCm39) using STAR (version 2.7.9a) aligner [146]. Downstream processing
782 of the data was performed using IDEP 1.0 [147, 148]. Gene counts were analyzed for
783 differentially expressed genes using DESeq2 [149]

784 Data availability

785 All of the data points collected on each mouse before and after the infection can
786 be found in the supplementary file (Table S2). Raw RNA sequencing files can be found
787 at Gene Expression Omnibus (GEO, submission in progress).

788 Acknowledgements

789 We thank Dr. Magnus Hook for providing the bacterial strain used in this study.
790 We also thank Dr. Karl Broman (University of Wisconsin) for helpful discussions and
791 troubleshooting problems in the rqtl2 google forum. We also thank Dr. Callie Kobayashi,
792 Dr. Joana Rocha, Mrs. Marissa Talamantes, Mr. Chris Bowden, Mr. Connor Mathis, and
793 Mrs. Kaya Mariello for technical assistance. Funding for this work was provided by the
794 Defense Advanced Research Projects Agency Grant Number D17AP00004.

Figure and Table descriptions

Main Figures

Fig 1: CC strains exhibit a diverse response to MRSA infection. After intravenous infection with MRSA USA300 as described in the Materials and Methods section, we show: A. survival time, B. percent weight change after infection, C. kidney colonization, and D. liver Colonization. CC strains are shown in the ascending order of survival. If survival was equal between two or more strains, strains are arranged in descending order of total bacterial load (the combination of colonization of all organs). Dots represent individual mice; black dots represent males; green dots represent females. The median and interquartile range are shown for each strain.

Fig 2: Sex differences in survival after MRSA infection. We present pooled data for the four strains that exhibited sex differences in survival: A. survival time, B. percent weight change after infection, C. colonization across organs, and D. pre-infection monocyte and red blood cell counts (U – Uninfected). Dots represent individual mice; black dots represent males; green dots represent females. Median with 95% Confidence Interval is shown for each strain. A, B, and D – Student's T-test and C – Mann-Whitney tests were performed to determine statistical significance (* = $P < 0.05$, ** = $P < 0.01$, *** = $P < 0.001$, **** = $P < 0.0001$)

Fig 3: Tissue damage correlates poorly with survival. A stacked bar plot showing the tissue damage score for five organs (Kidney = green, spleen = red, liver = yellow, heart = blue, lung = pink). Pathology in each tissue was scored by a blinded pathologist on a scale of 0 = no damage, to 4= severe damage.

817 **Fig 4: Several immune parameters differentiate the CC phenotypes.** A. Mean
818 neutrophil levels in uninfected mice (S – susceptible, T – Tolerant, R – Resistant). B.
819 Mean change in cytokine and chemokine levels after infection (Gray – Tolerant, Black –
820 Resistant). C. Top pathways from Gene Ontology (GO) enrichment analysis using
821 differentially expressed genes between tolerant and resistant strains. Lines represent
822 standard error of the mean. Student's T-test was performed to determine statistical
823 significance (* = P < 0.05, ** = P < 0.01, **** = P < 0.0001)

824 **Fig 5. Genomic regions involved in survival after MRSA infection.** LOD plots for
825 square root transformed survival phenotype (percentage of animals that survived at the
826 end of each day). A. Early survival (day 2 post-infection) peak on chromosome 18. B.
827 Late survival (day 7 post-infection) peak on chromosome 3. The dotted (Red – 95%,
828 Blue – 90%, Green – 85%) lines represent the significant LOD scores for 999
829 permutations.

830 **Fig 6. Strongest candidate genes on chromosome 18 for early survival.** A. Box plot
831 showing the founder allele contribution at the highest marker on the peak. Each dot
832 represents a strain, lines represent minimum to maximum. B. Genes with high-impact
833 variants shortlisted using the founder effect pattern. C. Mean kidney mRNA expression
834 values after infection (log-transformed). The number of animals is given within brackets.
835 Lines represent standard error of the mean values. Student's T-test was performed to
836 determine statistical significance (* = P < 0.05, ** = P < 0.01)

837 **Fig 7. Strongest candidate genes on chromosome 3 for late survival.** A. Box plot
838 showing the founder allele contribution at the highest marker on the peak. Each dot
839 represents a strain, lines represent minimum to maximum. B. Genes with high-impact

840 variants shortlisted using the founder effect pattern. C. Mean kidney mRNA expression
841 values after infection (log-transformed). The number of animals sequenced for each
842 founder allele is within the brackets. Lines represent standard error of the mean values.
843 Student's T-test was performed to determine statistical significance (* = P < 0.05, ** = P
844 < 0.01)

845 **Supplementary Figures**

846 **Fig S1: Colonization in other organs.** A. survival time. B. spleen colonization, C. heart
847 colonization. D. lung Colonization. Strains are in the ascending order of survival. If the
848 survival was equal, they are arranged in descending order of total organ colonization.
849 Dots represent individual mice; black dots represent males; green dots represent
850 females. The median and interquartile range are shown for each strain.

851 **Fig S2: Correlation with survival.** Heat map showing Spearman correlation 'R' values
852 between survival, weight change, organ colonization, and tissue damage scores.

853 **Fig S3. Representative images of organ histology scoring scheme.** Tissues were
854 sectioned and stained with H&E for scoring. Shows the 400X magnification of
855 representative scoring for all the organs.

856 **Fig S4: Time to deviation from the normal circadian pattern.** Plot showing the
857 number of animals that deviated from their normal pattern as identified by telemetry
858 system (machine - dot) vs. Laboratory worker (human - squares)

859 **Fig S5: Differentially expressed genes between tolerant and resistant strains**
860 **using DEseq2.** A. Venn diagram showing the number of upregulated and
861 downregulated genes in tolerant strains. B. Tree enrichment analysis using GO terms.

862 **Fig S6. Impact of sex on QTL regions.** LOD plots for square root transformed survival
863 phenotype excluding the four sex difference strains. A. Early survival. B. Late survival.
864 The dotted (Red – 99%, Blue – 95%, Green – 90%) lines represent the significant LOD
865 scores for 999 permutations.

866 **Fig S7. QTL plots for other phenotypes.** A. LOD plot for rank transformed relative
867 abundance values for significant genera. The dotted lines (Green – 85%, Blue – 90%,
868 Red – 95%) represent significant thresholds. B. Founder effect plot for the significant
869 chromosomes. C. Genotype X Phenotype plot for the highest SNP on the significant
870 chromosome.

871 **Fig S8. Circadian pattern for all mice involved in the study.** Blue line represents
872 temperature, black line represents activity and red line represents the time of infection.

873 **Fig S9. Temperature change after infection.** Change in temperature for each mouse
874 after infection (for 48 hours). The data is grouped by CC strain and colored lines in each
875 plot represent the strain averages.

876

877 **<u>Supplementary Tables</u>**

878 **Table S1: Mouse strains used in this study.** Number of mice, origin, and location of
879 breeding for all the mice used in the study.

880 **Table S2: Data associated with each mouse.** All the pre-infection and post-infection
881 data associated with each mouse in the study.

882 **Table S3: Tissue scoring matrix with descriptions.** The final score per organ
883 corresponds to the highest score assigned to a single category.

884 **Table S4: Shortlisted variants for survival peaks.** Sheet Chr_18 – high impact
885 variants on chromosome 3 for ESMI. Sheet Chr_3 – high impact variants on
886 chromosome 3 for LSMI.

887 **Table S5: QTL regions for other phenotypes**. At 85% (Sheet1) and 95 % (Sheet 2%)
888 significance threshold for 999 permutations.

889 **Table S6: Shortlisted variants for other phenotypes.** High impact variants in the QTL
890 regions listed on Table S5.

891

892 References

893

894 1. Lowy, F.D., *Staphylococcus aureus infections.* N Engl J Med, 1998. **339**(8): p.
895 520-32.
896 2. Krismer, B., et al., *The commensal lifestyle of Staphylococcus aureus and its*
897 *interactions with the nasal microbiota.* Nat Rev Microbiol, 2017. **15**(11): p. 675-
898 687.
899 3. Wertheim, H.F., et al., *The role of nasal carriage in Staphylococcus aureus*
900 *infections.* The Lancet infectious diseases, 2005. **5**(12): p. 751-762.
901 4. Laux, C., A. Peschel, and B. Krismer, *Staphylococcus aureus Colonization of the*
902 *Human Nose and Interaction with Other Microbiome Members.* Microbiol Spectr,
903 2019. **7**(2).
904 5. Haag, A.F., J.R. Fitzgerald, and J.R. Penadés, *Staphylococcus aureus in*
905 *Animals.* Microbiol Spectr, 2019. **7**(3).
906 6. Tong, S.Y., et al., *Staphylococcus aureus infections: epidemiology,*
907 *pathophysiology, clinical manifestations, and management.* Clin Microbiol Rev,
908 2015. **28**(3): p. 603-61.
909 7. Turner, N.A., et al., *Methicillin-resistant Staphylococcus aureus: an overview of*
910 *basic and clinical research.* Nat Rev Microbiol, 2019. **17**(4): p. 203-218.
911 8. Otto, M., *Community-associated MRSA: what makes them special?* Int J Med
912 Microbiol, 2013. **303**(6-7): p. 324-30.
913 9. Lee, A.S., et al., *Methicillin-resistant Staphylococcus aureus.* Nat Rev Dis
914 Primers, 2018. **4**: p. 18033.
915 10. Jevons, M.P., A.W. Coe, and M.T. Parker, *Methicillin resistance in staphylococci.*
916 Lancet, 1963. **1**(7287): p. 904-7.
917 11. Diekema, D.J., et al., *Continued emergence of USA300 methicillin-resistant*
918 *Staphylococcus aureus in the United States: results from a nationwide*
919 *surveillance study.* Infect Control Hosp Epidemiol, 2014. **35**(3): p. 285-92.
920 12. Planet, P.J., *Life After USA300: The Rise and Fall of a Superbug.* J Infect Dis,
921 2017. **215**(suppl_1): p. S71-S77.
922 13. Thurlow, L.R., G.S. Joshi, and A.R. Richardson, *Virulence strategies of the*
923 *dominant USA300 lineage of community-associated methicillin-resistant*
924 *Staphylococcus aureus (CA-MRSA).* FEMS Immunol Med Microbiol, 2012. **65**(1):
925 p. 5-22.
926 14. Kempker, R.R., et al., *Association of methicillin-resistant Staphylococcus aureus*
927 *(MRSA) USA300 genotype with mortality in MRSA bacteremia.* J Infect, 2010.
928 **61**(5): p. 372-81.
929 15. Kreisel, K.M., et al., *USA300 methicillin-resistant Staphylococcus aureus*
930 *bacteremia and the risk of severe sepsis: is USA300 methicillin-resistant*
931 *Staphylococcus aureus associated with more severe infections?* Diagn Microbiol
932 Infect Dis, 2011. **70**(3): p. 285-90.
933 16. Montgomery, C.P., et al., *Comparison of virulence in community-associated*
934 *methicillin-resistant Staphylococcus aureus pulsotypes USA300 and USA400 in*
935 *a rat model of pneumonia.* J Infect Dis, 2008. **198**(4): p. 561-70.

17. Cheung, G.Y., et al., *Role of the accessory gene regulator agr in community-associated methicillin-resistant Staphylococcus aureus pathogenesis.* Infect Immun, 2011. **79**(5): p. 1927-35.
18. Li, M., et al., *Evolution of virulence in epidemic community-associated methicillin-resistant Staphylococcus aureus.* Proc Natl Acad Sci U S A, 2009. **106**(14): p. 5883-8.
19. Shukla, S.K., W. Rose, and S.J. Schrodi, *Complex host genetic susceptibility to Staphylococcus aureus infections.* Trends Microbiol, 2015. **23**(9): p. 529-36.
20. Kim, H.K., D. Missiakas, and O. Schneewind, *Mouse models for infectious diseases caused by Staphylococcus aureus.* J Immunol Methods, 2014. **410**: p. 88-99.
21. Takeuchi, O., K. Hoshino, and S. Akira, *Cutting Edge: TLR2-Deficient and MyD88-Deficient Mice Are Highly Susceptible to Staphylococcus aureus Infection1.* The Journal of Immunology, 2000. **165**(10): p. 5392-5396.
22. Deshmukh, H.S., et al., *Critical role of NOD2 in regulating the immune response to Staphylococcus aureus.* Infect Immun, 2009. **77**(4): p. 1376-82.
23. von Kockritz-Blickwede, M., et al., *Immunological mechanisms underlying the genetic predisposition to severe Staphylococcus aureus infection in the mouse model.* Am J Pathol, 2008. **173**(6): p. 1657-68.
24. Yan, Q., et al., *Candidate genes on murine chromosome 8 are associated with susceptibility to Staphylococcus aureus infection in mice and are involved with Staphylococcus aureus septicemia in humans.* PLoS One, 2017. **12**(6): p. e0179033.
25. Yan, Q., et al., *Dusp3 and Psme3 are associated with murine susceptibility to Staphylococcus aureus infection and human sepsis.* PLoS Pathog, 2014. **10**(6): p. e1004149.
26. Ahn, S.H., et al., *Two genes on A/J chromosome 18 are associated with susceptibility to Staphylococcus aureus infection by combined microarray and QTL analyses.* PLoS Pathog, 2010. **6**(9): p. e1001088.
27. Noll, K.E., M.T. Ferris, and M.T. Heise, *The Collaborative Cross: A Systems Genetics Resource for Studying Host-Pathogen Interactions.* Cell Host Microbe, 2019. **25**(4): p. 484-498.
28. Threadgill, D.W., et al., *The collaborative cross: a recombinant inbred mouse population for the systems genetic era.* Ilar j, 2011. **52**(1): p. 24-31.
29. Churchill, G.A., et al., *The Collaborative Cross, a community resource for the genetic analysis of complex traits.* Nature genetics, 2004. **36**(11): p. 1133.
30. Srivastava, A., et al., *Genomes of the Mouse Collaborative Cross.* Genetics, 2017. **206**(2): p. 537-556.
31. Shorter, J.R., et al., *Whole Genome Sequencing and Progress Toward Full Inbreeding of the Mouse Collaborative Cross Population.* G3 Genes|Genomes|Genetics, 2019. **9**(5): p. 1303-1311.
32. Rasmussen, A.L., et al., *Host genetic diversity enables Ebola hemorrhagic fever pathogenesis and resistance.* Science, 2014. **346**(6212): p. 987-991.
33. Graham, J.B., et al., *Genetic diversity in the collaborative cross model recapitulates human West Nile virus disease outcomes.* MBio, 2015. **6**(3).

981 34. Ferris, M.T., et al., *Modeling host genetic regulation of influenza pathogenesis in*
982 *the collaborative cross.* PLoS Pathog, 2013. **9**(2): p. e1003196.
983 35. Xiong, H., et al., *Genomic profiling of collaborative cross founder mice infected*
984 *with respiratory viruses reveals novel transcripts and infection-related strain-*
985 *specific gene and isoform expression.* G3 (Bethesda), 2014. **4**(8): p. 1429-44.
986 36. Graham, J.B., et al., *Baseline T cell immune phenotypes predict virologic and*
987 *disease control upon SARS-CoV infection in Collaborative Cross mice.* PLoS
988 Pathog, 2021. **17**(1): p. e1009287.
989 37. Brinkmeyer-Langford, C.L., et al., *Host genetic background influences diverse*
990 *neurological responses to viral infection in mice.* Sci Rep, 2017. **7**(1): p. 12194.
991 38. Jensen, I.J., et al., *Novel Mouse Model of Murine Cytomegalovirus-Induced*
992 *Adaptive NK Cells.* Immunohorizons, 2022. **6**(1): p. 8-15.
993 39. Cartwright, H.N., et al., *Genetic diversity of collaborative cross mice enables*
994 *identification of novel rift valley fever virus encephalitis model.* PLoS Pathog,
995 2022. **18**(7): p. e1010649.
996 40. Smith, C.M., et al., *Tuberculosis Susceptibility and Vaccine Protection Are*
997 *Independently Controlled by Host Genotype.* mBio, 2016. **7**(5).
998 41. Smith, C.M., et al., *Host-pathogen genetic interactions underlie tuberculosis*
999 *susceptibility in genetically diverse mice.* Elife, 2022. **11**.
1000 42. Vered, K., et al., *Susceptibility to Klebsiella pneumonaie infection in collaborative*
1001 *cross mice is a complex trait controlled by at least three loci acting at different*
1002 *time points.* BMC Genomics, 2014. **15**: p. 865.
1003 43. Lorè, N.I., F.A. Iraqi, and A. Bragonzi, *Host genetic diversity influences the*
1004 *severity of Pseudomonas aeruginosa pneumonia in the Collaborative Cross*
1005 *mice.* BMC Genet, 2015. **16**: p. 106.
1006 44. Rogovskyy, A.S., et al., *The First Immunocompetent Mouse Model of Strictly*
1007 *Human Pathogen, Borrelia recurrentis.* Infect Immun, 2021. **89**(7): p. e0004821.
1008 45. Scoggin, K., et al., *Genetic background influences survival of infections with*
1009 *Salmonella enterica serovar Typhimurium in the Collaborative Cross.* PLoS
1010 Genet, 2022. **18**(4): p. e1010075.
1011 46. Scoggin, K., et al., *Elucidating Mechanisms of Tolerance to Salmonella*
1012 *Typhimurium across Long-Term Infections Using the Collaborative Cross.* mBio,
1013 2022. **13**(4): p. e0112022.
1014 47. Alugupalli, K.R., et al., *Identification of collaborative cross mouse strains*
1015 *permissive to Salmonella enterica serovar Typhi infection.* Sci Rep, 2023. **13**(1):
1016 p. 393.
1017 48. Ali, R.A., et al., *Platelets Mediate Host Defense against Staphylococcus aureus*
1018 *through Direct Bactericidal Activity and by Enhancing Macrophage Activities.* J
1019 Immunol, 2017. **198**(1): p. 344-351.
1020 49. Yun, S.H., et al., *Platelet Activation: The Mechanisms and Potential Biomarkers.*
1021 Biomed Res Int, 2016. **2016**: p. 9060143.
1022 50. Broman, K.W., et al., *R/qtl2: Software for Mapping Quantitative Trait Loci with*
1023 *High-Dimensional Data and Multiparent Populations.* Genetics, 2019. **211**(2): p.
1024 495-502.

1025 51. Vincent, M., et al., *QTLViewer: an interactive webtool for genetic analysis in the*
1026 *Collaborative Cross and Diversity Outbred mouse populations.* G3
1027 Genes|Genomes|Genetics, 2022. **12**(8).
1028 52. Blake, J.A., et al., *Mouse Genome Database (MGD): Knowledgebase for mouse-*
1029 *human comparative biology.* Nucleic Acids Res, 2021. **49**(D1): p. D981-d987.
1030 53. Clarridge, J.E., 3rd, et al., *Impact of strain typing methods on assessment of*
1031 *relationship between paired nares and wound isolates of methicillin-resistant*
1032 *Staphylococcus aureus.* J Clin Microbiol, 2013. **51**(1): p. 224-31.
1033 54. Howden, B.P., et al., *Staphylococcus aureus host interactions and adaptation.*
1034 Nature Reviews Microbiology, 2023.
1035 55. Cheng, A.G., et al., *Genetic requirements for Staphylococcus aureus abscess*
1036 *formation and persistence in host tissues.* FASEB J, 2009. **23**(10): p. 3393-404.
1037 56. Wong, C.H., et al., *Nucleation of platelets with blood-borne pathogens on Kupffer*
1038 *cells precedes other innate immunity and contributes to bacterial clearance.*
1039 Nature immunology, 2013. **14**(8): p. 785-792.
1040 57. Pollitt, E.J., et al., *Staphylococcus aureus infection dynamics.* PLoS pathogens,
1041 2018. **14**(6): p. e1007112.
1042 58. Dias, S.P., M.C. Brouwer, and D. van de Beek, *Sex and Gender Differences in*
1043 *Bacterial Infections.* Infect Immun, 2022. **90**(10): p. e0028322.
1044 59. Fish, E.N., *The X-files in immunity: sex-based differences predispose immune*
1045 *responses.* Nat Rev Immunol, 2008. **8**(9): p. 737-44.
1046 60. Harbarth, S., et al., *Evaluating the probability of previously unknown carriage of*
1047 *MRSA at hospital admission.* The American journal of medicine, 2006. **119**(3): p.
1048 275. e15-275. e23.
1049 61. Laupland, K.B., et al., *The changing epidemiology of Staphylococcus aureus*
1050 *bloodstream infection: a multinational population-based surveillance study.*
1051 Clinical microbiology and infection, 2013. **19**(5): p. 465-471.
1052 62. Kaasch, A.J., et al., *Staphylococcus aureus bloodstream infection: a pooled*
1053 *analysis of five prospective, observational studies.* Journal of Infection, 2014.
1054 **68**(3): p. 242-251.
1055 63. Maclayton, D.O., et al., *Case-control study of the relationship between MRSA*
1056 *bacteremia with a vancomycin MIC of 2 µg/mL and risk factors, costs, and*
1057 *outcomes in inpatients undergoing hemodialysis.* Clinical therapeutics, 2006.
1058 **28**(8): p. 1208-1216.
1059 64. Mansur, N., et al., *Does sex affect 30-day mortality in Staphylococcus aureus*
1060 *bacteremia?* Gender medicine, 2012. **9**(6): p. 463-470.
1061 65. Smit, J., et al., *Gender differences in the outcome of community-acquired*
1062 *Staphylococcus aureus bacteraemia: a historical population-based cohort study.*
1063 Clinical Microbiology and Infection, 2017. **23**(1): p. 27-32.
1064 66. Paulsen, J., et al., *Epidemiology and outcome of Staphylococcus aureus*
1065 *bloodstream infection and sepsis in a Norwegian county 1996–2011: an*
1066 *observational study.* BMC infectious diseases, 2015. **15**(1): p. 1-10.
1067 67. Kubica, M., et al., *A potential new pathway for Staphylococcus aureus*
1068 *dissemination: the silent survival of S. aureus phagocytosed by human*
1069 *monocyte-derived macrophages.* PloS one, 2008. **3**(1): p. e1409.

68. Pidwill, G.R., et al., *The Role of Macrophages in Staphylococcus aureus Infection.* Front Immunol, 2020. **11**: p. 620339.
69. Croize, J., et al., *Improved identification of Staphylococcus aureus using a new agglutination test. Results of an international study.* Apmis, 1993. **101**(6): p. 487-91.
70. Wilkerson, M., et al., *Comparison of five agglutination tests for identification of Staphylococcus aureus.* J Clin Microbiol, 1997. **35**(1): p. 148-51.
71. Shin, P.K., et al., *Characteristics of new Staphylococcus aureus-RBC adhesion mechanism independent of fibrinogen and IgG under hydrodynamic shear conditions.* Am J Physiol Cell Physiol, 2005. **289**(3): p. C727-34.
72. Gianquinto, E., et al., *Interaction of human hemoglobin and semi-hemoglobins with the Staphylococcus aureus hemophore IsdB: a kinetic and mechanistic insight.* Scientific Reports, 2019. **9**(1): p. 18629.
73. Spaan, A.N., et al., *Staphylococcus aureus Targets the Duffy Antigen Receptor for Chemokines (DARC) to Lyse Erythrocytes.* Cell Host Microbe, 2015. **18**(3): p. 363-70.
74. Skaar, E.P., et al., *Iron-source preference of Staphylococcus aureus infections.* Science, 2004. **305**(5690): p. 1626-8.
75. Bundgaard, H., et al., *Long-term outcomes of partial oral treatment of endocarditis.* N Engl J Med, 2019. **10**.
76. Iversen, K., et al., *Partial oral versus intravenous antibiotic treatment of endocarditis.* New England Journal of Medicine, 2019. **380**(5): p. 415-424.
77. Parker, D., *Humanized Mouse Models of Staphylococcus aureus Infection.* Front Immunol, 2017. **8**: p. 512.
78. Bor, D.H., et al., *Infective Endocarditis in the U.S., 1998–2009: A Nationwide Study.* PLOS ONE, 2013. **8**(3): p. e60033.
79. Federspiel, J.J., et al., *Increasing US rates of endocarditis with Staphylococcus aureus: 1999-2008.* Archives of internal medicine, 2012. **172**(4): p. 363-365.
80. Gibson, G.W., et al., *Development of a mouse model of induced Staphylococcus aureus infective endocarditis.* Comparative medicine, 2007. **57**(6): p. 563-569.
81. Liesenborghs, L., et al., *Staphylococcus aureus endocarditis: distinct mechanisms of bacterial adhesion to damaged and inflamed heart valves.* Eur Heart J, 2019. **40**(39): p. 3248-3259.
82. Wasi, F. and J. Shuter, *Primary bacterial infection of the myocardium.* Front Biosci, 2003. **8**: p. s228-31.
83. LeLeiko, R.M., D.J. Bower, and C.P. Larsen, *MRSA-associated bacterial myocarditis causing ruptured ventricle and tamponade.* Cardiology, 2008. **111**(3): p. 188-90.
84. Jariwala, P., et al., *Myocardial abscess secondary to staphylococcal septicemia: diagnosis with 3D echocardiography.* Indian Heart J, 2013. **65**(1): p. 124-5.
85. Lee, L.-N., et al., *Characteristics and local risk factors of community-acquired and health-care-associated Staphylococcus aureus pneumonia.* Scientific Reports, 2022. **12**(1): p. 18670.
86. Dell'Isola, G.B., et al., *Noncontact Body Temperature Measurement: Uncertainty Evaluation and Screening Decision Rule to Prevent the Spread of COVID-19.* Sensors (Basel), 2021. **21**(2).

1116 87. Lippi, G., et al., *Is body temperature mass screening a reliable and safe option*
1117 *for preventing COVID-19 spread?* Diagnosis (Berl), 2021. **9**(2): p. 195-198.
1118 88. Dzien, C., et al., *Covid-19 screening: are forehead temperature measurements*
1119 *during cold outdoor temperatures really helpful?* Wien Klin Wochenschr, 2021.
1120 **133**(7-8): p. 331-335.
1121 89. Sharif Nia, H., et al., *Clinical accuracy and agreement between tympanic and*
1122 *forehead body temperature measurements for screening of patients with COVID-*
1123 *19.* J Clin Nurs, 2022. **31**(21-22): p. 3272-3285.
1124 90. Ngcobo, S., et al., *Pre-infection plasma cytokines and chemokines as predictors*
1125 *of HIV disease progression.* Sci Rep, 2022. **12**(1): p. 2437.
1126 91. Spaan, A.N., et al., *Neutrophils versus Staphylococcus aureus: a biological tug of*
1127 *war.* Annu Rev Microbiol, 2013. **67**: p. 629-50.
1128 92. Bouma, G., et al., *Recent advances in the understanding of genetic defects of*
1129 *neutrophil number and function.* Br J Haematol, 2010. **151**(4): p. 312-26.
1130 93. Andrews, T. and K.E. Sullivan, *Infections in patients with inherited defects in*
1131 *phagocytic function.* Clin Microbiol Rev, 2003. **16**(4): p. 597-621.
1132 94. Lakshman, R. and A. Finn, *Neutrophil disorders and their management.* J Clin
1133 Pathol, 2001. **54**(1): p. 7-19.
1134 95. Pollitt, E.J.G., et al., *Staphylococcus aureus infection dynamics.* PLoS Pathog,
1135 2018. **14**(6): p. e1007112.
1136 96. Rigby, K.M. and F.R. DeLeo, *Neutrophils in innate host defense against*
1137 *Staphylococcus aureus infections.* Seminars in Immunopathology, 2012. **34**(2): p.
1138 237-259.
1139 97. Hamilton, J.A., *GM-CSF in inflammation.* Journal of Experimental Medicine,
1140 2019. **217**(1).
1141 98. Ali, A., et al., *IL-1 Receptor Antagonist Treatment Aggravates Staphylococcal*
1142 *Septic Arthritis and Sepsis in Mice.* PLoS One, 2015. **10**(7): p. e0131645.
1143 99. Miller, L.S., et al., *MyD88 mediates neutrophil recruitment initiated by IL-1R but*
1144 *not TLR2 activation in immunity against Staphylococcus aureus.* Immunity, 2006.
1145 **24**(1): p. 79-91.
1146 100. Cohen, T.S. and A.S. Prince, *Bacterial pathogens activate a common*
1147 *inflammatory pathway through IFNλ regulation of PDCD4.* PLoS pathogens,
1148 2013. **9**(10): p. e1003682.
1149 101. Henningsson, L., et al., *Interleukin 15 Mediates Joint Destruction in*
1150 *Staphylococcus Aureus Arthritis.* The Journal of Infectious Diseases, 2012.
1151 **206**(5): p. 687-696.
1152 102. van Drongelen, V., et al., *Reduced filaggrin expression is accompanied by*
1153 *increased Staphylococcus aureus colonization of epidermal skin models.* Clin
1154 Exp Allergy, 2014. **44**(12): p. 1515-24.
1155 103. Boisson, B., *The genetic basis of pneumococcal and staphylococcal infections:*
1156 *inborn errors of human TLR and IL-1R immunity.* Human Genetics, 2020. **139**(6):
1157 p. 981-991.
1158 104. Krishna, S. and L.S. Miller, *Innate and adaptive immune responses against*
1159 *Staphylococcus aureus skin infections.* Seminars in Immunopathology, 2012.
1160 **34**(2): p. 261-280.

1161 105. Hultgren, O.H., L. Svensson, and A. Tarkowski, *Critical role of signaling through*
1162 *IL-1 receptor for development of arthritis and sepsis during Staphylococcus*
1163 *aureus infection.* J Immunol, 2002. **168**(10): p. 5207-12.
1164 106. Wortzel, I. and R. Seger, *The ERK Cascade: Distinct Functions within Various*
1165 *Subcellular Organelles.* Genes Cancer, 2011. **2**(3): p. 195-209.
1166 107. von Kriegsheim, A., et al., *Cell fate decisions are specified by the dynamic ERK*
1167 *interactome.* Nat Cell Biol, 2009. **11**(12): p. 1458-64.
1168 108. Lucas, R.M., L. Luo, and J.L. Stow, *ERK1/2 in immune signalling.* Biochem Soc
1169 Trans, 2022. **50**(5): p. 1341-1352.
1170 109. Kopczynski, M., et al., *Selective Extracellular Signal-Regulated Kinase 1/2*
1171 *(ERK1/2) Inhibition by the SCH772984 Compound Attenuates In Vitro and In*
1172 *Vivo Inflammatory Responses and Prolongs Survival in Murine Sepsis Models.*
1173 Int J Mol Sci, 2021. **22**(19).
1174 110. Zhao, S., et al., *TGF-β1 promotes Staphylococcus aureus adhesion to and*
1175 *invasion into bovine mammary fibroblasts via the ERK pathway.* Microb Pathog,
1176 2017. **106**: p. 25-29.
1177 111. Chen, Y., et al., *Identification of a novel variant in N-cadherin associated with*
1178 *dilated cardiomyopathy.* Front Med (Lausanne), 2022. **9**: p. 944950.
1179 112. Mayosi, B.M., et al., *Identification of Cadherin 2 (CDH2) Mutations in*
1180 *Arrhythmogenic Right Ventricular Cardiomyopathy.* Circ Cardiovasc Genet, 2017.
1181 **10**(2).
1182 113. Ye, J.Z., et al., *Reevaluation of genetic variants previously associated with*
1183 *arrhythmogenic right ventricular cardiomyopathy integrating population-based*
1184 *cohorts and proteomics data.* Clin Genet, 2019. **96**(6): p. 506-514.
1185 114. Kostetskii, I., et al., *Induced deletion of the N-cadherin gene in the heart leads to*
1186 *dissolution of the intercalated disc structure.* Circ Res, 2005. **96**(3): p. 346-54.
1187 115. Herman-Bausier, P., et al., *Staphylococcus aureus Fibronectin-Binding Protein A*
1188 *Mediates Cell-Cell Adhesion through Low-Affinity Homophilic Bonds.* mBio, 2015.
1189 **6**(3): p. e00413-15.
1190 116. Pfeffer, S.R., *NPC intracellular cholesterol transporter 1 (NPC1)-mediated*
1191 *cholesterol export from lysosomes.* J Biol Chem, 2019. **294**(5): p. 1706-1709.
1192 117. Pentchev, P.G., *Niemann–Pick C research from mouse to gene.* Biochimica et
1193 Biophysica Acta (BBA) - Molecular and Cell Biology of Lipids, 2004. **1685**(1): p.
1194 3-7.
1195 118. Hendrikx, T., et al., *Lysosomal cholesterol accumulation: driver on the road to*
1196 *inflammation during atherosclerosis and non-alcoholic steatohepatitis.* Obes Rev,
1197 2014. **15**(5): p. 424-33.
1198 119. Xu, X., et al., *Lysosomal cholesterol accumulation in macrophages leading to*
1199 *coronary atherosclerosis in CD38(-/-) mice.* J Cell Mol Med, 2016. **20**(6): p. 1001-
1200 13.
1201 120. Carette, J.E., et al., *Ebola virus entry requires the cholesterol transporter*
1202 *Niemann–Pick C1.* Nature, 2011. **477**(7364): p. 340-343.
1203 121. Morales-Tenorio, M., et al., *Potential pharmacological strategies targeting the*
1204 *Niemann-Pick C1 receptor and Ebola virus glycoprotein interaction.* European
1205 Journal of Medicinal Chemistry, 2021. **223**: p. 113654.

1206 122. Tang, Y., et al., *Deficiency of niemann-pick type C-1 protein impairs release of*
1207 *human immunodeficiency virus type 1 and results in Gag accumulation in late*
1208 *endosomal/lysosomal compartments.* Journal of virology, 2009. **83**(16): p. 7982-
1209 7995.
1210 123. Sainz, B., et al., *Identification of the Niemann-Pick C1–like 1 cholesterol*
1211 *absorption receptor as a new hepatitis C virus entry factor.* Nature Medicine,
1212 2012. **18**(2): p. 281-285.
1213 124. Wichit, S., et al., *Imipramine Inhibits Chikungunya Virus Replication in Human*
1214 *Skin Fibroblasts through Interference with Intracellular Cholesterol Trafficking.* Sci
1215 Rep, 2017. **7**(1): p. 3145.
1216 125. Houben, T., et al., *Hematopoietic Npc1 mutation shifts gut microbiota composition*
1217 *in Ldlr(-/-) mice on a high-fat, high-cholesterol diet.* Sci Rep, 2019. **9**(1): p. 14956.
1218 126. Schwerd, T., et al., *Impaired antibacterial autophagy links granulomatous*
1219 *intestinal inflammation in Niemann-Pick disease type C1 and XIAP deficiency*
1220 *with NOD2 variants in Crohn's disease.* Gut, 2017. **66**(6): p. 1060-1073.
1221 127. Prajsnar, T.K., et al., *The autophagic response to Staphylococcus aureus*
1222 *provides an intracellular niche in neutrophils.* Autophagy, 2021. **17**(4): p. 888-902.
1223 128. Dai, Y., et al., *Heterogeneous Vancomycin-Intermediate Staphylococcus aureus*
1224 *Uses the VraSR Regulatory System to Modulate Autophagy for Increased*
1225 *Intracellular Survival in Macrophage-Like Cell Line RAW264.7.* Front Microbiol,
1226 2019. **10**: p. 1222.
1227 129. O'Keeffe, K.M., et al., *Manipulation of Autophagy in Phagocytes Facilitates*
1228 *Staphylococcus aureus Bloodstream Infection.* Infect Immun, 2015. **83**(9): p.
1229 3445-57.
1230 130. Astle, W.J., et al., *The Allelic Landscape of Human Blood Cell Trait Variation and*
1231 *Links to Common Complex Disease.* Cell, 2016. **167**(5): p. 1415-1429.e19.
1232 131. Busse, D.C., et al., *Interferon-Induced Protein 44 and Interferon-Induced Protein*
1233 *44-Like Restrict Replication of Respiratory Syncytial Virus.* J Virol, 2020. **94**(18).
1234 132. Jiang, H., et al., *IFI44L as a Forward Regulator Enhancing Host Antituberculosis*
1235 *Responses.* J Immunol Res, 2021. **2021**: p. 5599408.
1236 133. DeDiego, M.L., L. Martinez-Sobrido, and D.J. Topham, *Novel Functions of IFI44L*
1237 *as a Feedback Regulator of Host Antiviral Responses.* J Virol, 2019. **93**(21).
1238 134. Holden, M.T., et al., *Complete genomes of two clinical Staphylococcus aureus*
1239 *strains: evidence for the rapid evolution of virulence and drug resistance.* Proc
1240 Natl Acad Sci U S A, 2004. **101**(26): p. 9786-91.
1241 135. Highlander, S.K., et al., *Subtle genetic changes enhance virulence of methicillin*
1242 *resistant and sensitive Staphylococcus aureus.* BMC Microbiol, 2007. **7**: p. 99.
1243 136. Lee, H.S., et al., *Comparative Study of the Difference in Behavior of the*
1244 *Accessory Gene Regulator (Agr) in USA300 and USA400 Community-*
1245 *Associated Methicillin-Resistant Staphylococcus aureus (CA-MRSA).* J Microbiol
1246 Biotechnol, 2021. **31**(8): p. 1060-1068.
1247 137. Jones, M.B., et al., *Genomic and transcriptomic differences in community*
1248 *acquired methicillin resistant Staphylococcus aureus USA300 and USA400*
1249 *strains.* BMC Genomics, 2014. **15**: p. 1145.
1250 138. Redi, D., et al., *Staphylococcus aureus vaccine preclinical and clinical*
1251 *development: current state of the art.* New Microbiol, 2018. **41**(3): p. 208-213.

139. Miller, L.S., et al., *Development of a vaccine against Staphylococcus aureus invasive infections: Evidence based on human immunity, genetics and bacterial evasion mechanisms.* FEMS Microbiol Rev, 2020. **44**(1): p. 123-153.
140. Bogue, M.A., et al., *Mouse Phenome Database: towards a more FAIR-compliant and TRUST-worthy data repository and tool suite for phenotypes and genotypes.* Nucleic Acids Res, 2023. **51**(D1): p. D1067-d1074.
141. Cunningham, F., et al., *Ensembl 2022.* Nucleic Acids Res, 2022. **50**(D1): p. D988-d995.
142. Krueger, F., *Taking appropriate QC measures for RRBS-type or other -Seq applications with Trim Galore!* Github, 2019.
143. Kechin, A., et al., *cutPrimers: A New Tool for Accurate Cutting of Primers from Reads of Targeted Next Generation Sequencing.* J Comput Biol, 2017. **24**(11): p. 1138-1143.
144. *FastQC*. 2015.
145. Andrews, S., *FastQC: a quality control tool for high throughput sequence data*. 2010, Babraham Bioinformatics, Babraham Institute, Cambridge, United Kingdom.
146. Dobin, A., et al., *STAR: ultrafast universal RNA-seq aligner.* Bioinformatics, 2013. **29**(1): p. 15-21.
147. Ge, S.X., E.W. Son, and R. Yao, *iDEP: an integrated web application for differential expression and pathway analysis of RNA-Seq data.* BMC Bioinformatics, 2018. **19**(1): p. 534.
148. Ge, X., *iDEP Web Application for RNA-Seq Data Analysis.* Methods Mol Biol, 2021. **2284**: p. 417-443.
149. Love, M.I., W. Huber, and S. Anders, *Moderated estimation of fold change and dispersion for RNA-seq data with DESeq2.* Genome Biol, 2014. **15**(12): p. 550.

Fig 1

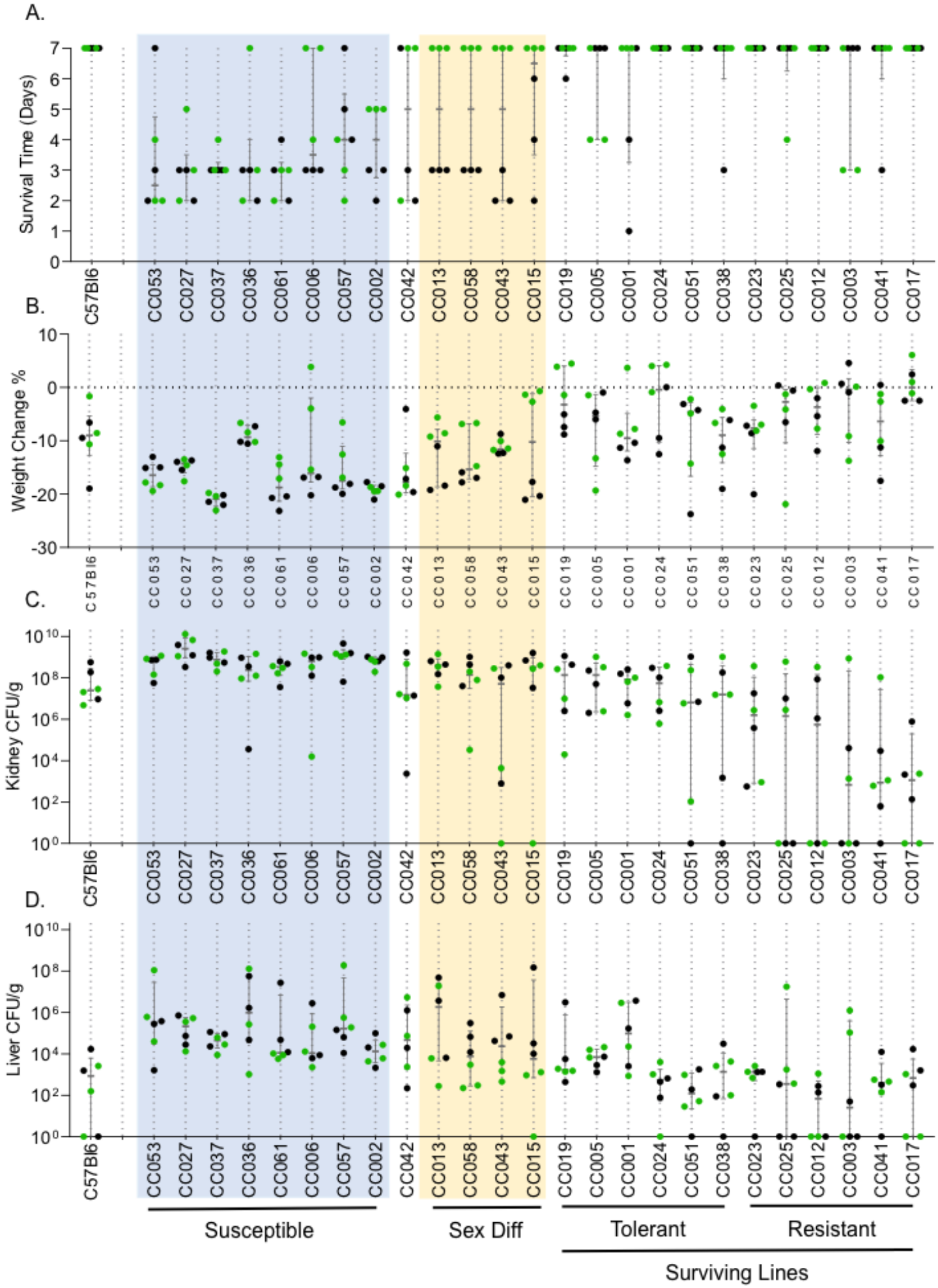
A.
Survival Time (Days)
B.
Weight Change %
C.
Kidney CFU/g
D.
Liver CFU/g
C57Bl6
CC053
CC027
CC037
CC036
CC061
CC006
CC057
CC002
CC042
CC013
CC058
CC043
CC015
CC019
CC005
CC001
CC024
CC051
CC038
CC023
CC025
CC012
CC003
CC041
CC017
Susceptible
Sex Diff
Tolerant
Resistant
Surviving Lines

Fig 2

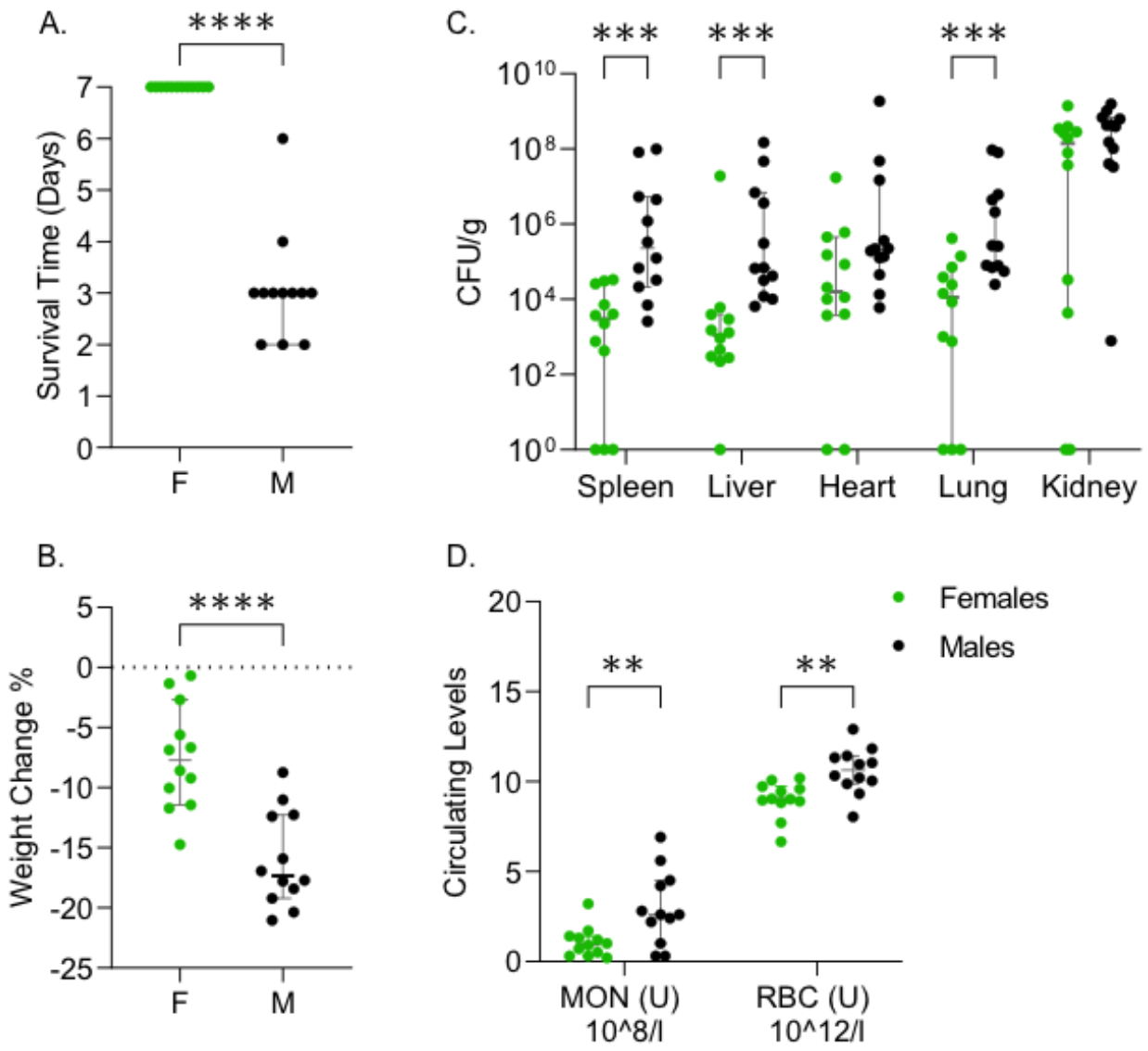
A.
****
Survival Time (Days)
0
1
2
3
4
5
6
7
F
M
B.
****
Weight Change %
5
0
-5
-10
-15
-20
-25
F
M
C.
***
***
***
CFU/g
10^{10}
10^{8}
10^{6}
10^{4}
10^{2}
10^{0}
Spleen
Liver
Heart
Lung
Kidney
D.
Circulating Levels
20
15
10
5
0
**
**
MON (U)
10^8/l
RBC (U)
10^12/l
Females
Males

Fig 3

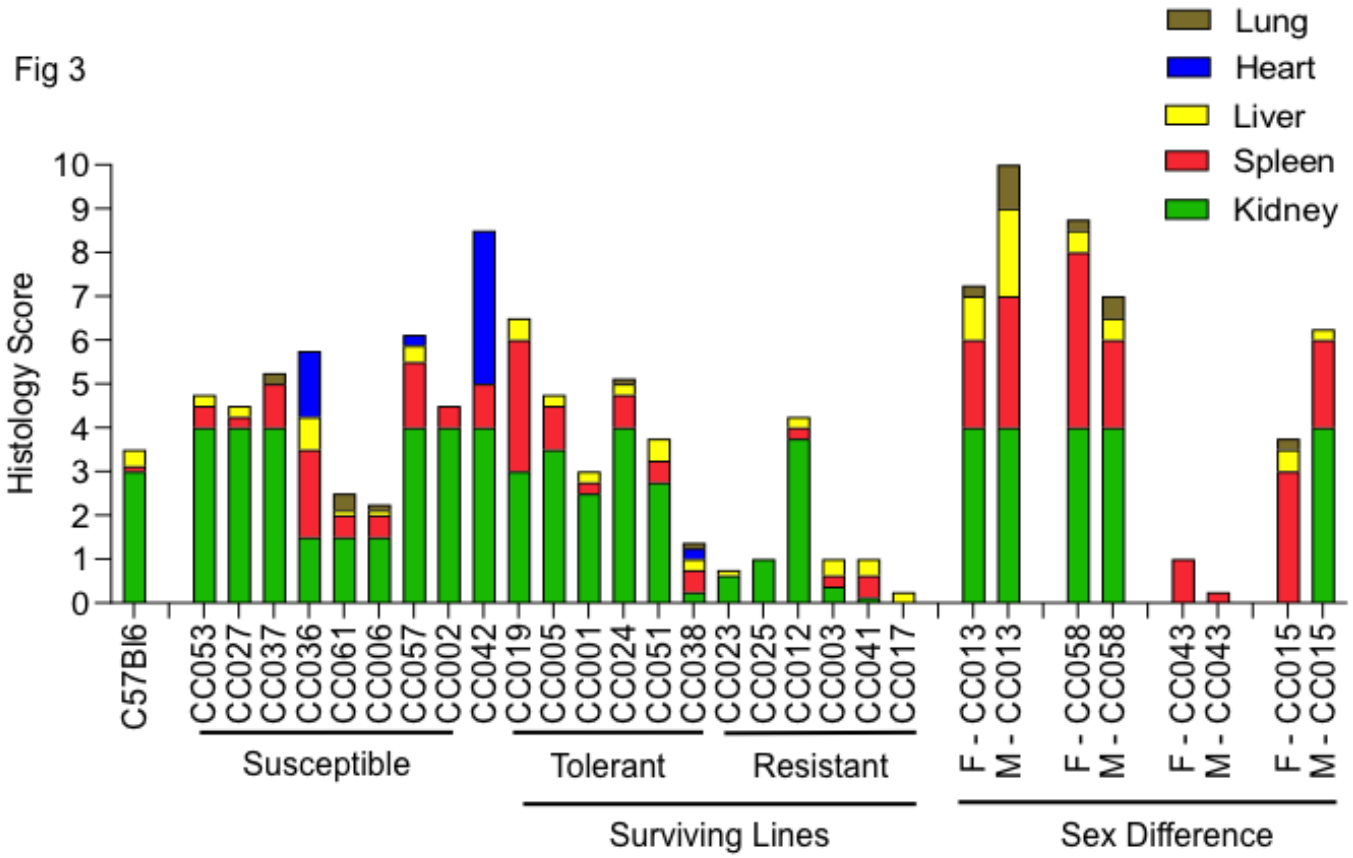
Lung
Heart
Liver
Spleen
Kidney
Histology Score
0
1
2
3
4
5
6
7
8
9
10
C57Bl6
CC053
CC027
CC037
CC036
CC061
CC006
CC057
CC002
CC042
CC019
CC005
CC001
CC024
CC051
CC038
CC023
CC025
CC012
CC003
CC041
CC017
F - CC013
M - CC013
F - CC058
M - CC058
F - CC043
M - CC043
F - CC015
M - CC015
Susceptible
Tolerant
Resistant
Surviving Lines
Sex Difference

Fig 4

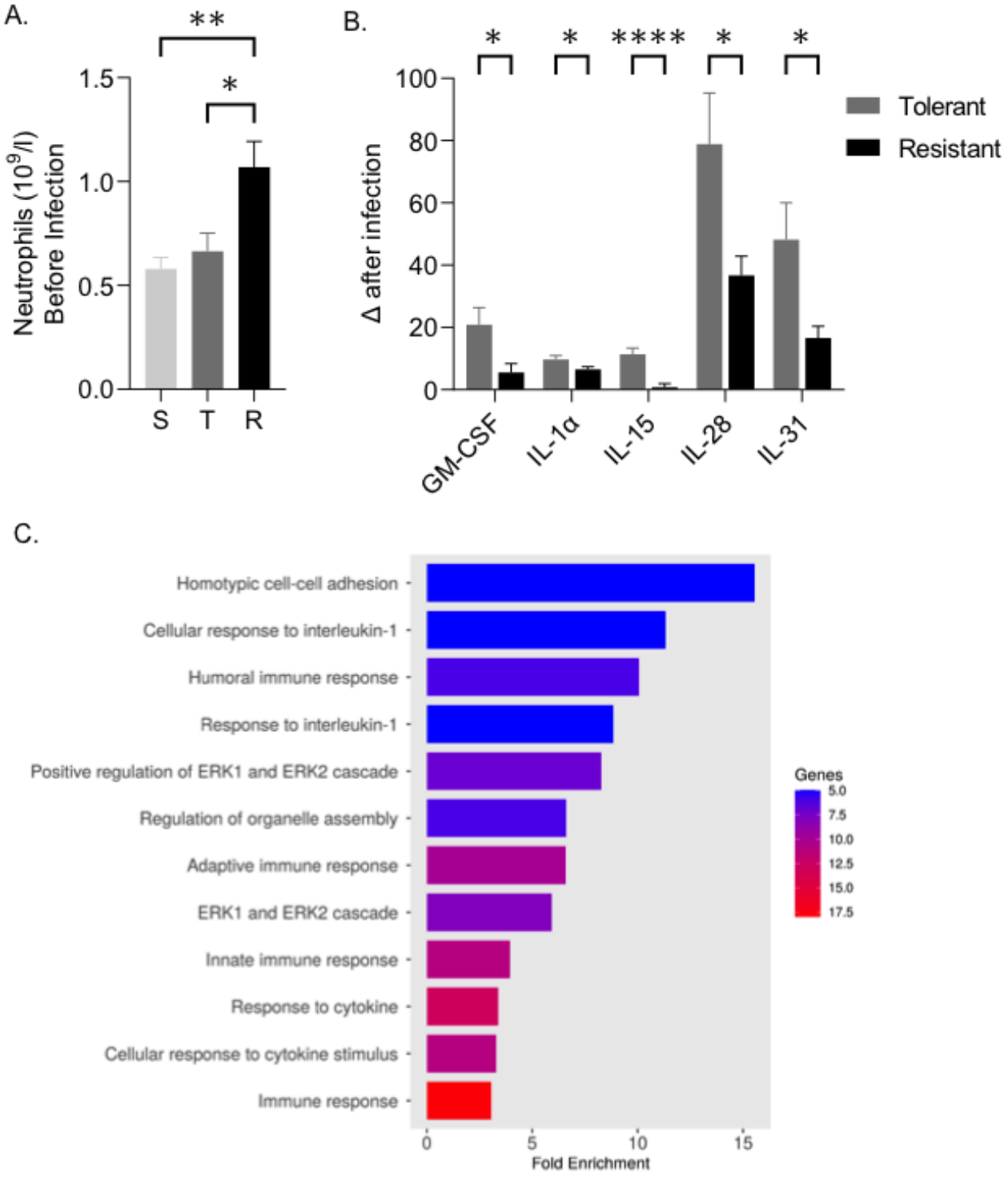
A.
**
*
1.5
1.0
0.5
0.0
Neutrophils (10^9/l)
Before Infection
S
T
R
B.
*
*
****
*
*
100
80
60
40
20
0
Δ after infection
Tolerant
Resistant
GM-CSF
IL-1α
IL-15
IL-28
IL-31
C.
Homotypic cell-cell adhesion
Cellular response to interleukin-1
Humoral immune response
Response to interleukin-1
Positive regulation of ERK1 and ERK2 cascade
Regulation of organelle assembly
Adaptive immune response
ERK1 and ERK2 cascade
Innate immune response
Response to cytokine
Cellular response to cytokine stimulus
Immune response
0
5
10
15
Fold Enrichment
Genes
5.0
7.5
10.0
12.5
15.0
17.5

Fig 5

A.

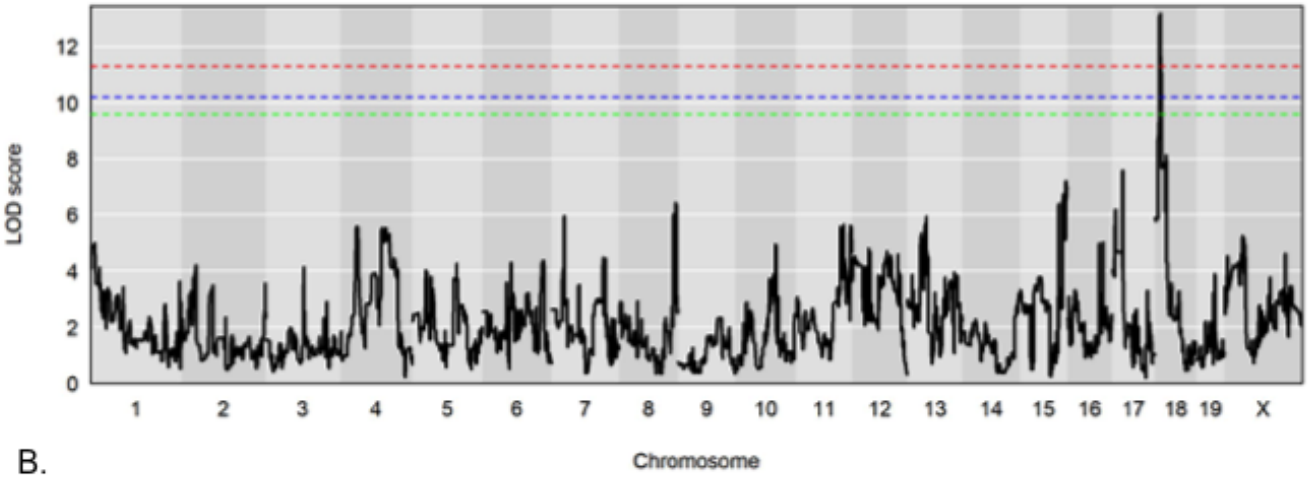
LOD score
0
2
4
6
8
10
12
1 2 3 4 5 6 7 8 9 10 11 12 13 14 15 16 17 18 19 X
Chromosome

B.

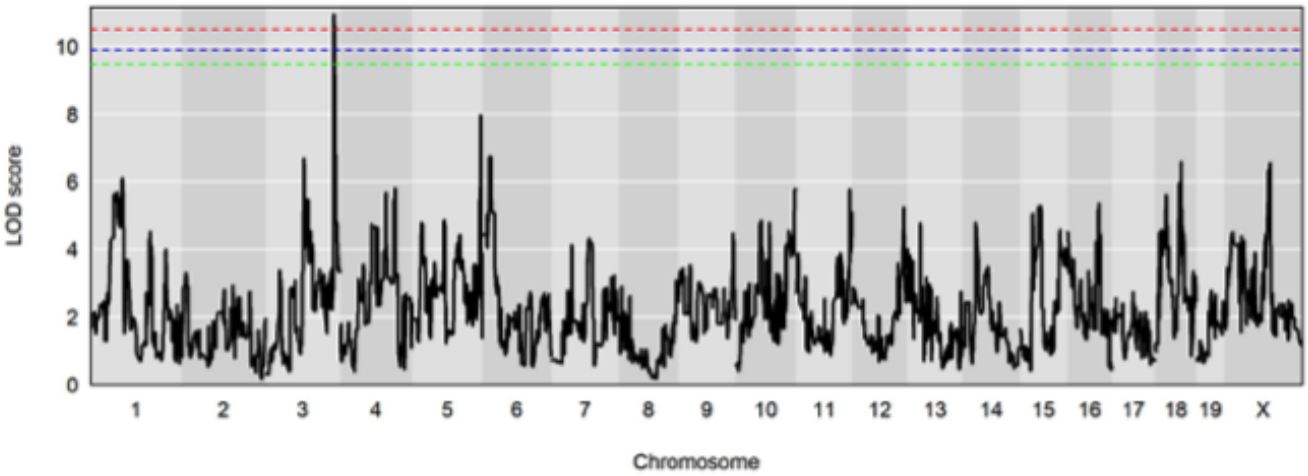
LOD score
0
2
4
6
8
10
1 2 3 4 5 6 7 8 9 10 11 12 13 14 15 16 17 18 19 X
Chromosome

Fig 6

A.

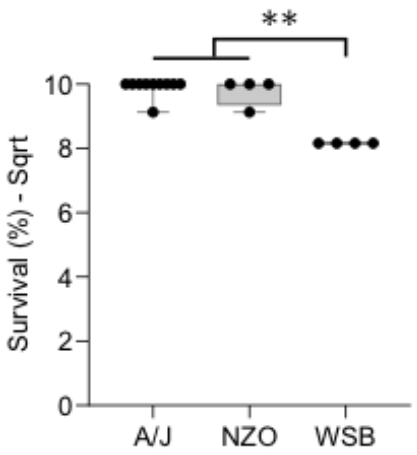

B.

GENE	SNP_ID	A/J	NZO	WSB	Cons
Npc1	rs30985329	A	A	T	missense
Lama3	rs51262081	C	C	G	missense
Cabyr	rs49718484	A	A	G	missense
Osbpl1a	rs48171054	T	T	C	missense
Psma8	rs31135735	A	A	G	missense
Kctd1	rs226935597	G	G	T	missense
Cdh2	rs243156099	C	C	T	splice region

C.

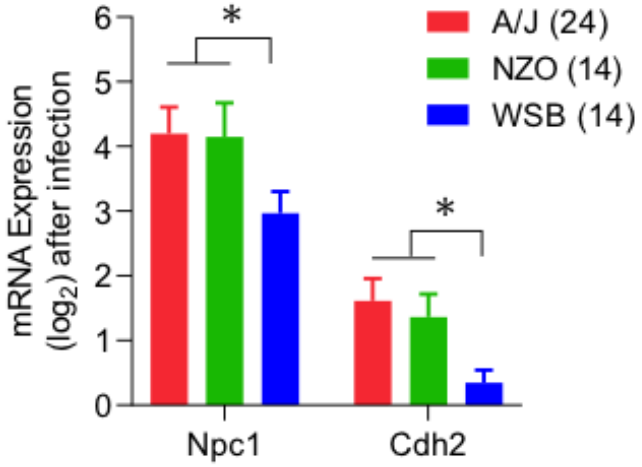

Fig 7

A.

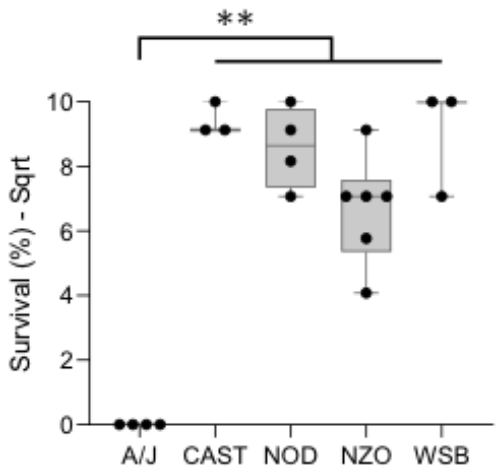

B.

GENE	SNP_ID	A/J	CAST	NOD	NZO	WSB	Cons
Uox	rs31217970	T	C	C	C	C	synonymous
Adgrl4	rs30505737	T	A	A	A	A	splice region
Ifi44	rs48866215	A.	G	G	G	G	missense
Ifi44l	rs31149902	G	A	A	A	A	synonymous
Miga1	rs31134017	G	T	T	T	T	missense
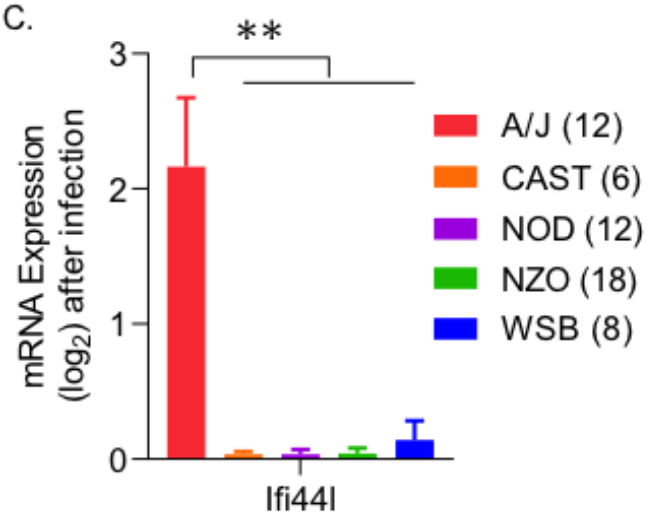
C.